

Opposite physiological and pathological mTORC1-mediated roles of the CB1 receptor in regulating renal tubular function

Liad Hinden ¹, Majdoleen Ahmad¹, Sharleen Hamad¹, Alina Nemirovski¹, Gergő Szanda², Sandra Glasmacher³, Aviram Kogot-Levin⁴, Rinat Abramovitch ^{5,6}, Bernard Thorens ⁷, Jürg Gertsch ³, Gil Leibowitz ⁴ & Joseph Tam ¹✉

Activation of the cannabinoid-1 receptor (CB₁R) and the mammalian target of rapamycin complex 1 (mTORC1) in the renal proximal tubular cells (RPTCs) contributes to the development of diabetic kidney disease (DKD). However, the CB₁R/mTORC1 signaling axis in the kidney has not been described yet. We show here that hyperglycemia-induced endocannabinoid/CB₁R stimulation increased mTORC1 activity, enhancing the transcription of the facilitative glucose transporter 2 (GLUT2) and leading to the development of DKD in mice; this effect was ameliorated by specific RPTCs ablation of GLUT2. Conversely, CB₁R maintained the normal activity of mTORC1 by preventing the cellular excess of amino acids during normoglycemia. Our findings highlight a novel molecular mechanism by which the activation of mTORC1 in RPTCs is tightly controlled by CB₁R, either by enhancing the reabsorption of glucose and inducing kidney dysfunction in diabetes or by preventing amino acid uptake and maintaining normal kidney function in healthy conditions.

¹Obesity and Metabolism Laboratory, The Institute for Drug Research, School of Pharmacy, Faculty of Medicine, The Hebrew University of Jerusalem, Jerusalem, Israel. ²Department of Physiology, Semmelweis University, Budapest, Hungary. ³Institute of Biochemistry and Molecular Medicine, University of Bern, Bern, Switzerland. ⁴Diabetes Unit and Endocrine Service, Hadassah-Hebrew University Medical Center, Jerusalem, Israel. ⁵The Wohl Institute for Translational Medicine, Hadassah-Hebrew University Medical Center, Jerusalem, Israel. ⁶The Goldyne Savad Institute of Gene Therapy, Hadassah-Hebrew University Medical Center, Jerusalem, Israel. ⁷Center for Integrative Genomics, University of Lausanne, Lausanne, Switzerland.

✉email: yossi.tam@mail.huji.ac.il

Diabetes is a chronic disease that is now reaching epidemic proportions¹, and has been described as a catalyst for a number of conditions, most notably cardiovascular disease, retinopathy, and diabetic kidney disease (DKD). The latter affects approximately 30% of patients with diabetes, and it is strongly associated with morbidity and mortality². DKD is manifested by glomerular hypertrophy, transient hyperfiltration, albuminuria, kidney fibrosis, and ultimately a progressive decline in the glomerular filtration rate³. Recently, a paradigm shift in our understanding of kidney dysfunction in diabetic patients has emerged, indicating that tubulopathy precedes glomerular alterations^{4,5}. The renal proximal tubular cells (RPTCs) are uniquely susceptible to a variety of metabolic and hemodynamic factors associated with diabetes, especially to hyperglycemia. In fact, glucose entry into RPTCs is insulin-independent, making these cells particularly sensitive to the deleterious effects of chronic hyperglycemia in diabetic patients, that in turn, may lead to enhanced O₂ consumption and increased hypoxic tubular damage⁵. During normoglycemia, however, the RPTCs account for 25% of whole-body gluconeogenesis, and play a key role in glucose⁶ and amino acid⁷ reabsorption, thus maintaining adequate blood glucose levels and metabolic homeostasis.

Both the cannabinoid-1 receptor (CB₁R) and the mammalian target of rapamycin complex 1 (mTORC1) are considered as mediators of the “Thrifty Phenotype”, evolutionarily designed for consuming and storing energy when an excess of nutrients is available^{8–10}. This effect is of great importance when mammals prepare themselves for a “time of need”. However, this advantage becomes a double-edged sword for humans in our modern world of satiation and contentment, where overnutrition contributes significantly to the increased prevalence of diabetes and obesity. Both CB₁R and mTORC1 were shown to be involved in kidney pathologies under hyperglycemic conditions^{11–16}. For instance, CB₁R has been shown to be upregulated in podocytes, mesangial cells, and RPTCs in diabetes, and its pharmacological inhibition by CB₁R antagonists ameliorates diabetes-induced kidney dysfunction, inflammation, and fibrosis^{17–25}. Hyperglycemia also activates mTORC1 in these cells and its inhibition ameliorates oxidative stress, endoplasmic reticulum stress, epithelial-to-mesenchymal transition, inflammation, and fibrosis^{26–34}. Stimulation of mTORC1 in response to nutrient flux contributes to tubule-interstitial fibrosis^{16,31,35–37} and apoptosis³⁸; therefore, mTORC1 has been suggested as a potential therapeutic target for DKD³⁹. In fact, a positive association between CB₁R and mTORC1 activities has been previously described in the central nervous system^{40–44}. In contrast, peripheral CB₁R antagonism has been shown to decrease glucose-stimulated insulin secretion (GSIS) and gastric ghrelin secretion via activation of mTORC1^{45,46}. Interestingly, activation of mTORC1 has been shown to stimulate GSIS under diabetic conditions by elevating the protein levels of the facilitative glucose transporter GLUT2⁴⁷.

A growing body of evidence indicates that hyperglycemia induces changes in glucose transport via GLUT2 and may negatively affect kidney function and the associated tubulo-interstitial changes seen in DKD^{48,49}. In contrast to the reduced expression of GLUT2 in pancreatic β cells in different models of diabetes^{50–52}, its levels in RPTCs rise in diabetic patients⁵³ as well as in murine models of diabetes and obesity^{54–56}. Plasma or luminal glucose concentrations are known to regulate its expression and/or translocation⁵⁷, accounting for the deleterious effects of hyperglycemia on the proximal tubule. Recently, we have demonstrated that diabetes-induced upregulation in kidney GLUT2 expression and dynamic translocation is mitigated by peripheral pharmacological blockade or genetic deletion of CB₁R in RPTCs, and that it reduces glucose reabsorption and prevents the development of DKD²⁵. However, there are several fundamental open questions

that should be addressed: What are the cellular mechanisms by which hyperglycemia activates CB₁R? How do CB₁Rs specifically regulate the transcriptional levels of GLUT2? And what is the explicit role of GLUT2 in RPTCs in the development of DKD? Addressing these important questions will eventually advance our understanding of the interaction of CB₁R and GLUT2 in the development of DKD. Based on the key roles of CB₁R and mTORC1 in whole-body energy utilization, and their similar involvement in the pathogenesis of DKD, we aimed to determine whether these two pathways interact in the proximal tubules and affect kidney homeostasis in health and disease. Here, we show a profound inactivation of mTORC1 signaling and, consequently, downregulation of GLUT2 in diabetic mice lacking CB₁R specifically in RPTCs; these molecular events were associated with preserved kidney function in the diabetic mice. Furthermore, we show that hyperglycemia specifically enhances the endocannabinoid (eCB)/CB₁R ‘tone’ in RPTCs, promoting a cascade of molecular events that activate mTORC1, which in turn, triggers transcriptional changes in the GLUT2 promoter, ultimately enhancing its expression. On the other hand, non-diabetic mice lacking CB₁R in RPTCs display enhanced mTORC1 activation as a result of elevated amino acid transport, causing morphological abnormalities in the kidney and renal dysfunction. These observations reveal the critical role of CB₁R in maintaining normal mTORC1 activity in RPTCs both under pathological and physiological conditions. Finally, we demonstrate that a specific reduction in GLUT2 expression in RPTCs is sufficient to protect diabetic mice from developing DKD, emphasizing this transporter’s role in regulating renal glucose homeostasis and the pathogenesis of DKD. Overall, our data describe for the first time an opposing CB₁R/mTORC1 signaling axis in healthy and diseased kidney.

Results

CB₁R in the RPTCs plays a key role in DKD development. Overactivation of the kidney eCB/CB₁R system contributes to the development of DKD, and its blockade by CB₁R antagonists ameliorates kidney dysfunction in diabetic mice^{17–25}. To specifically decipher the importance of CB₁R in RPTCs in DKD, we crossed RPTC-CB₁R^{-/-} mice²¹ with insulin-deficient diabetic *Akita*^{Ins2+/C96Y} mice, thereby generating diabetic mice lacking CB₁R in RPTCs (Supplementary Fig. 1a–e). The metabolic phenotype of *Akita*-RPTC-CB₁R^{-/-} mice and of *Akita*-RPTC-CB₁R^{+/+} controls did not differ and they exhibited similar reduction of body weight, hyperglycemia along with hypoinsulinemia without affecting pancreatic weight (Supplementary Fig. 1f–k). Nevertheless, the *Akita*-RPTC-CB₁R^{-/-} mice were protected from the deleterious effects of hyperglycemia on their kidneys, exhibiting reduced kidney-to-body weight, urine excretion-to-water consumption, and albumin-to-creatinine (ACR) ratios, reduced proteinuria, albuminuria, and urinary excretion of kidney injury marker 1 (KIM1), as well as improved creatinine clearance (CCr; Fig. 1a–g). The amelioration of kidney function in the *Akita*-RPTC-CB₁R^{-/-} mice compared to *Akita* was associated with improved kidney morphological appearance (Fig. 1h–k), along with decreased expression of markers of kidney injury, inflammation, and fibrosis (Fig. 1l–n). Taken together, these findings highlight that RPTC-CB₁Rs play an important role in the pathophysiology of DKD.

Both GLUT2 and mTORC1 are regulated by proximal tubule CB₁R. Molecularly, the absence of RPTC CB₁R in *Akita* diabetic mice resulted in the inhibition of kidney mTORC1 activity, manifested by the remarkable reduction in ribosomal protein S6 phosphorylation (pS6; Fig. 2a, d) and associated well with the reduced expression of its upstream regulator phosphorylated active AKT

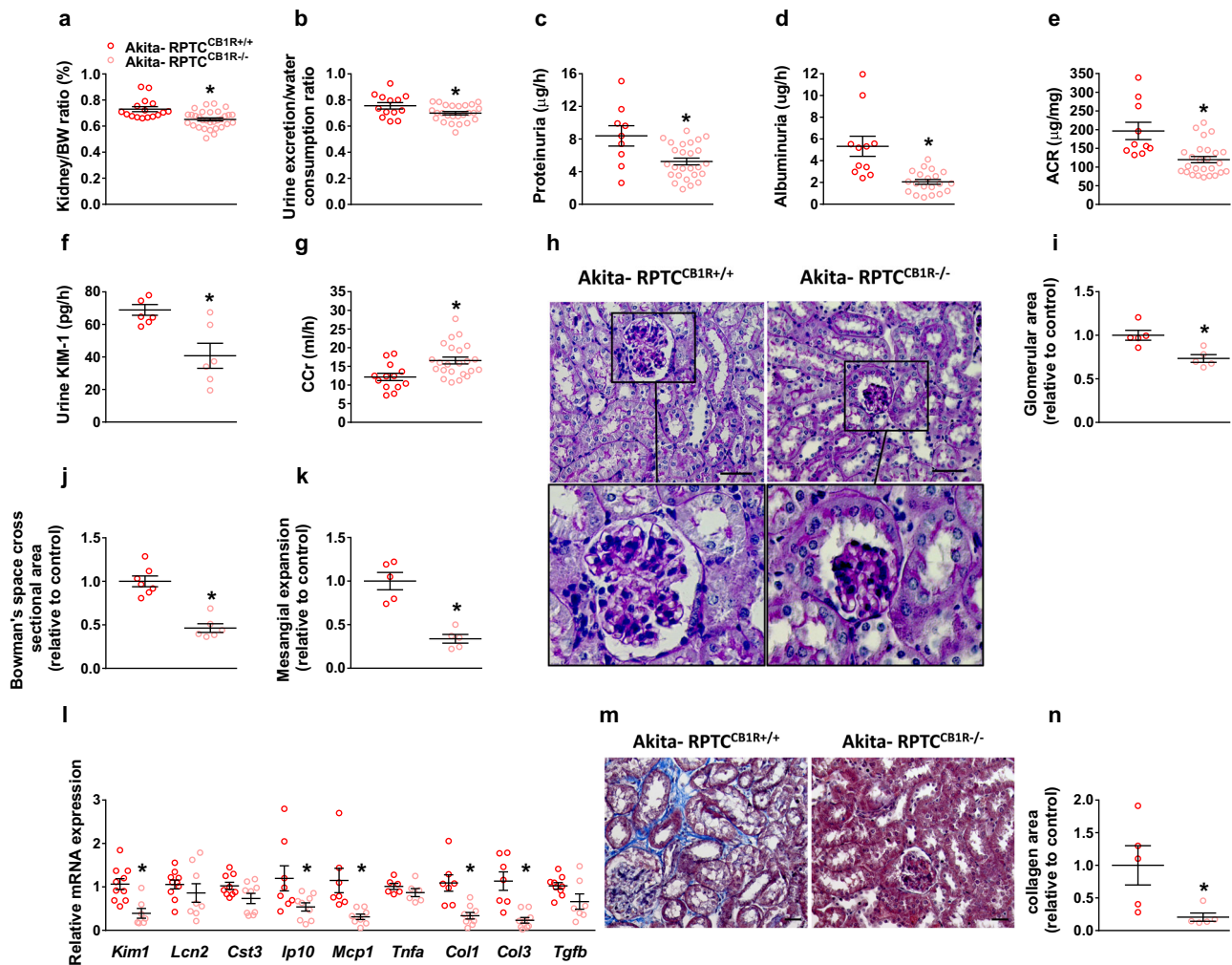
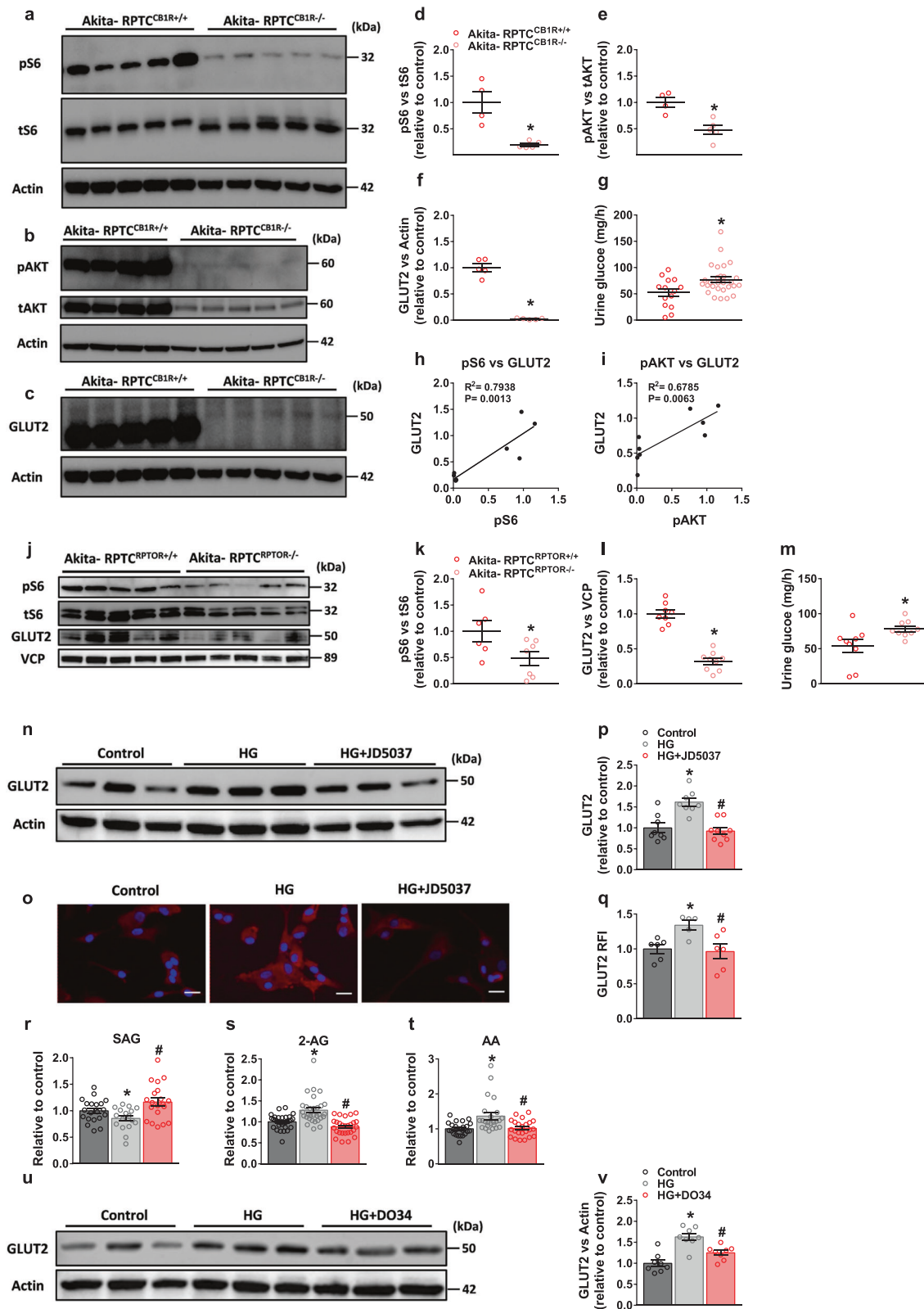


Fig. 1 Specific CB_1R deletion in RPTCs protects Akita mice from developing DKD. **a** Kidney-to-body weight ratio of 16-week-old Akita diabetic mice. $n = 16$ mice for Akita-RPTC $^{CB1R+/+}$, $n = 31$ mice for Akita-RPTC $^{CB1R-/-}$ ($*P = 0.0005$). **b** Urine excretion-to-water consumption ratio of 16-week-old Akita diabetic mice. $n = 10$ mice for Akita-RPTC $^{CB1R+/+}$, $n = 22$ mice for Akita-RPTC $^{CB1R-/-}$ ($*P = 0.0274$). **c** Proteinuria in 16-week-old Akita diabetic mice. $n = 9$ mice for Akita-RPTC $^{CB1R+/+}$, $n = 26$ mice for Akita-RPTC $^{CB1R-/-}$ ($*P = 0.0039$). **d** Albuminuria in 16-week-old Akita diabetic mice. $n = 11$ mice for Akita-RPTC $^{CB1R+/+}$, $n = 17$ mice for Akita-RPTC $^{CB1R-/-}$ ($*P = 0.0274$). **e** Urine albumin-to-creatinine ratio (ACR) in 16-week-old Akita diabetic mice. $n = 10$ mice for Akita-RPTC $^{CB1R+/+}$, $n = 26$ mice for Akita-RPTC $^{CB1R-/-}$ ($*P = 0.0004$). **f** Urine KIM-1 levels in 16-week-old Akita diabetic mice. $n = 7$ mice for Akita-RPTC $^{CB1R+/+}$, $n = 6$ mice for Akita-RPTC $^{CB1R-/-}$ ($*P = 0.0046$). **g** Creatinine clearance (CCr) in 16-week-old Akita diabetic mice. $n = 13$ mice for Akita-RPTC $^{CB1R+/+}$, $n = 23$ mice for Akita-RPTC $^{CB1R-/-}$ ($*P = 0.0040$). **h** Representative PAS staining of the kidney, 40 \times magnification, scale bar: 50 μ m. **i** Glomerular area quantification (at least 10 glomeruli per mouse). $n = 5$ mice for Akita-RPTC $^{CB1R+/+}$, $n = 5$ mice for Akita-RPTC $^{CB1R-/-}$ ($*P = 0.0061$). **j** Bowman's space cross-sectional area quantification (at least 10 glomeruli per mouse). $n = 7$ mice for Akita-RPTC $^{CB1R+/+}$, $n = 6$ mice for Akita-RPTC $^{CB1R-/-}$ ($*P < 0.0001$). **k** Mesangial expansion quantification (at least 10 glomeruli per mouse). $n = 5$ mice for Akita-RPTC $^{CB1R+/+}$, $n = 5$ mice for Akita-RPTC $^{CB1R-/-}$ ($*P = 0.0003$). **l** qPCR analyses of renal injury markers: *Kim1*, *Lcn2*, and *Cst3*, inflammatory markers: *Ip10*, *Mcp1*, and *Tnfa*, and fibrogenic markers: *Col1*, *Col3*, and *Tgfb*. $n = 7$ mice per group ($*P < 0.0363$). **m** Representative Masson's trichrome staining of the kidney, 40 \times magnification, scale bar: 50 μ m. **n** Collagen deposition positive area quantification. $n = 5$ mice per group ($*P = 0.0323$). Data represent the mean \pm SEM and were analyzed by Unpaired Two-tailed Student's t-test. Source data are provided as a Source Data file.

(Fig. 2b, e). Importantly, GLUT2 expression was decreased in the Akita-RPTC- $CB_1R^{-/-}$ mice (Fig. 2c, f), concomitant with a significant increase in glycosuria (Fig. 2g). In fact, significant positive correlations between pS6 or pAKT and GLUT2 expression were found (Fig. 2h, i). Conversely, inducing acute CB_1R activation by administering WIN-55,212 to WT mice increased kidney mTORC1 activity and elevated GLUT2 expression levels (Supplementary Fig. 2a–c). These results are in agreement with our previous findings, demonstrating that peripheral pharmacological blockade of CB_1R ameliorates DKD in Akita and in streptozotocin (STZ)-induced diabetic mice via downregulating GLUT2 expression and its dynamic translocation²⁵.

To further study the link between mTORC1 and GLUT2, we utilized the same breeding paradigm to either inactivate or overactivate mTORC1 signaling in RPTCs by generating Akita-RPTC-RPTOR $^{-/-}$ and WT-RPTC-TSC $^{-/-}$ mice⁵⁸, respectively. The regulatory-associated protein of mTOR (RPTOR) is essential for mTORC1 activation and its absence in the RPTCs of diabetic mice resulted in reduced pS6 levels (Fig. 2j, k), which were associated with reduced GLUT2 expression (Fig. 2j, l) and resulted in a significant increase in glycosuria (Fig. 2m). These changes were associated with improved kidney function and fibrosis, as recently reported by us in mice with partial inhibition of mTORC1 in RPTCs⁵⁸. On the other hand, the absence of the



tuberous sclerosis complex (TSC) in RPTCs results in constant mTORC1 activation and elevated GLUT2 protein expression (Supplementary Fig. 2d–f), effects that are associated with tubular dysfunction, peritubular fibrosis, albuminuria, and kidney dysfunction⁵⁸. Moreover, in diabetic mice that lack CB₁R, on the one hand, and have constant mTORC1 activity in

their RPTCs, on the other hand (Akita-RPTC-CB₁R^{-/-}-TSC^{+/-} animals), the beneficial effects of CB₁R deletion in enhancing glucosuria, reducing proteinuria and albuminuria, and improving CCr were completely abrogated by partial deletion of TSC (Supplementary Fig. 3a–h), further supporting the regulatory role of CB₁R in mTORC1 signaling and kidney homeostasis.

Fig. 2 RPTC CB₁R regulates mTORC1 and GLUT2. **a, d** Immunoblotting analysis and quantification of pS6 (S235/236) in kidney lysates from Akita-RPTC^{CB₁R+/+} and Akita-RPTC^{CB₁R-/-} diabetic mice. $n = 4$ mice for Akita-RPTC^{CB₁R+/+}, $n = 5$ mice for Akita-RPTC^{CB₁R-/-} ($*P = 0.0032$). **b, e** Immunoblotting analysis and quantification of pAKT (S473) in kidney lysates from Akita-RPTC^{CB₁R+/+} and Akita-RPTC^{CB₁R-/-} diabetic mice. $n = 4$ mice for Akita-RPTC^{CB₁R+/+}, $n = 5$ mice for Akita-RPTC^{CB₁R-/-} ($*P = 0.0056$). **c, f** Immunoblotting analysis and quantification of GLUT2 in kidney lysates from Akita-RPTC^{CB₁R+/+} and Akita-RPTC^{CB₁R-/-} diabetic mice. $n = 5$ mice per group ($*P < 0.0001$). **g** Urinary glucose levels in diabetic mice. $n = 14$ mice for Akita-RPTC^{CB₁R+/+}, $n = 28$ mice for Akita-RPTC^{CB₁R-/-} ($*P = 0.0123$). **h, i** Correlation analysis between pS6 or pAKT and GLUT2 protein expression levels (**h**, $P = 0.0013$; **i**, $P = 0.0063$). **j** Representative immunoblots for pS6 and GLUT2 in kidney lysates from Akita-RPTC^{RPTOR+/+} and Akita-RPTC^{RPTOR-/-} diabetic mice. $n = 5$ mice per group. **k** Immunoblotting analysis for pS6 in kidney lysates. $n = 6$ mice for Akita-RPTC^{RPTOR+/+}, $n = 7$ mice for Akita-RPTC^{RPTOR-/-} ($*P = 0.0475$). **l** Immunoblotting analysis for GLUT2 in kidney lysates. $n = 8$ mice for Akita-RPTC^{RPTOR+/+}, $n = 9$ mice for Akita-RPTC^{RPTOR-/-} ($*P < 0.0001$). **m** Urinary glucose levels in Akita-RPTC^{RPTOR+/+} and Akita-RPTC^{RPTOR-/-} diabetic mice. $n = 9$ mice per group ($*P = 0.0271$). **n, p** Representative immunoblots of GLUT2 in hRPTCs treated with HG (30 mM) or HG + JD5037 (100 nM) for 24 h. $n = 8$ for Control and HG groups, $n = 9$ for HG + JD5037 ($*P = 0.0010$, $\#P < 0.0001$). **o, q** Representative GLUT2 immunofluorescence staining of primary hRPTCs treated with HG (30 mM) or HG + JD5037 (100 nM) for 24 h and quantification. 10 \times magnification, scale bar: 100 μ m. $n = 6$ for Control and HG + JD5037 groups, $n = 5$ for HG group ($*P = 0.0049$, $\#P = 0.0189$). **r** LC-MS/MS quantification of SAG in primary hRPTCs treated with HG (30 mM) or HG + JD5037 (100 nM) for 1 h. $n = 20$ biological replicates for the control group, $n = 17$ for HG group, $n = 20$ for HG + JD group ($*P = 0.0467$, $\#P = 0.0025$). **s** LC-MS/MS quantification of 2-AG in primary hRPTCs treated with HG (30 mM) or HG + JD5037 (100 nM) for 1 h. $n = 31$ for Control, $n = 30$ for HG group, $n = 27$ for HG + JD group ($*P < 0.0001$, $\#P < 0.0001$). **t** LC-MS/MS quantification of AA in primary hRPTCs treated with HG (30 mM) or HG + JD5037 (100 nM) for 1 h. $n = 24$ for Control and HG groups, $n = 23$ for HG + JD group ($*P = 0.0010$, $\#P = 0.0026$). **u, v** Representative immunoblots of GLUT2 in hRPTCs treated with HG (30 mM) or HG + DO34 (100 nM) for 24 h. $n = 8$ per group ($*P < 0.0001$, $\#P = 0.0025$). Data represent the mean \pm SEM and were analyzed by Unpaired Two-tailed Student's t-test or one-way ANOVA followed by Tukey test (one-sided). In **b–j** $*P < 0.05$ relative to the corresponding Akita-RPTC^{CB₁R+/+} or Akita-RPTC^{RPTOR+/+} control groups. In **l–q** $*P < 0.05$ relative to the corresponding control group. $\#P < 0.05$ relative to the HG-treated group. Source data are provided as a Source Data file.

Hyperglycemia increases endocannabinoid ‘tone’ in RPTCs.

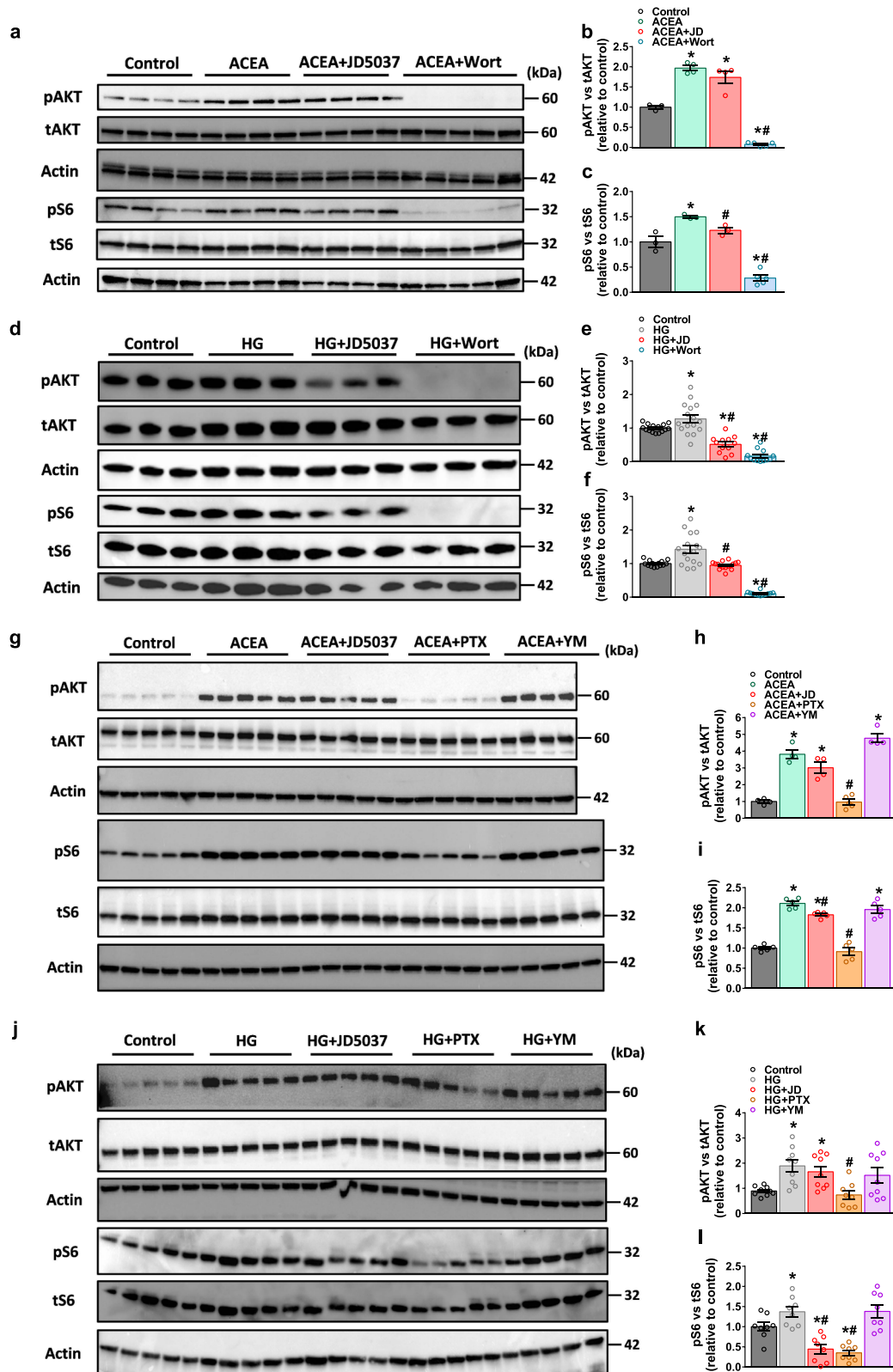
Next, we aimed to determine whether acute exposure of human primary RPTCs to hyperglycemic conditions induces an elevation in GLUT2 expression in a CB₁R-dependent manner. Indeed, GLUT2 protein levels were upregulated by the high glucose (HG) levels and normalized with CB₁R antagonism (Fig. 2n–q). The HG-induced increase in GLUT2 expression was associated with enhanced 2-arachidonoylglycerol (2-AG) synthesis, manifested by reduced levels of the precursor 1-stearoyl-2-arachidonoyl-*sn*-glycerol (SAG) and elevated 2-AG and arachidonic acid (AA) levels (Fig. 2r–t and Supplementary Fig. 4a–f). However, no changes were found in the expression of the two isoforms of diacylglycerol lipase (DAGL), the rate-limiting enzyme in the biosynthesis of 2-AG (Supplementary Fig. 5a–e). In fact, inhibiting its activity by DO34 in HG-treated hRPTCs normalized the elevated GLUT2 protein levels (Fig. 2u, v), suggesting a vicious cycle by which hyperglycemia induces CB₁R reactivation by 2-AG production and subsequently increases GLUT2 expression through activation of the CB₁R/mTORC1 signaling pathway.

CB₁R modulates mTORC1 via a Gi-PI3K-dependent signaling pathway. As a G protein-coupled receptor (GPCR), CB₁R may affect mTORC1 activity and consequently, GLUT2 via several cellular signaling pathways. In fact, CB₁R-induced phosphorylation of AKT is known to be regulated upstream via the activation (phosphorylation) of PIP2 by phosphoinositide 3-kinases (PI3K) induced through the $\beta\gamma$ subunit of GPCR^{59–61}. Investigating the effect of CB₁R activation either by the synthetic cannabinoid arachidonyl-2'-chloroethylamide (ACEA) or by hyperglycemia in hRPTCs revealed that both conditions increased pAKT and pS6 in a PI3K-dependent manner, since their effects were completely prevented by the PI3K inhibitor wortmannin and partially by the CB₁R inverse agonist JD5037 (Fig. 3a–f). CB₁R G-protein coupling may be biased according to the means of its activation; it stabilizes its conformation either towards Gi- or Gq-coupled signaling^{62,63}. Therefore, we next examined which of the two possible molecular events is triggered by CB₁R agonism and hyperglycemia. We found that pretreatment of RPTCs with the Gi inhibitor, pertussis toxin (PTX), but not with the Gq inhibitor, YM254890, abolished the effect of CB₁R activation or HG on mTORC1 activation (Fig. 3g–l). Collectively, these results suggest

that CB₁R activates mTORC1 and increases GLUT2 expression in Gi- and PI3K-dependent manner.

GLUT2 transcription is directly regulated by CB₁R and mTORC1. Next, we determined the molecular mechanism by which CB₁R/mTORC1 axis affects GLUT2. To that end, we cloned the hGLUT2 promoter into a *Firefly* reporter plasmid (pGL3-GLUT2), which was then transfected into HEK-293 cells together with a *Renilla* plasmid for the purpose of normalization (T2; Supplementary Fig. 6a–c). Exposing these cells to HG resulted in elevated transcription of GLUT2, indicated by the increased luminescence relative response ratio (RRR; Fig. 4a, Supplementary Fig. 6d). To further evaluate the direct effect of CB₁R on GLUT2 transcription, we utilized the CB₁R-TK-d64 plasmid, in which a CB₁R lacking the first 64 amino acids of the long N-terminal tail⁶⁴ is expressed under the human herpes virus tyrosine kinase (TK) promoter (Supplementary Fig. 6b, c, e, f). First, we validated that CB₁R protein expression levels are not downregulated by co-transfecting the cells with pGL3-P1 and *Renilla* plasmids (Supplementary Fig. 6g, h). Then, we found that co-transfection of pGL3-GLUT2 with CB₁R-TK-d64 (T3) further enhanced GLUT2 transcription (Fig. 4b). In addition, blockade of CB₁R (by JD5037) normalized ACEA- or HG-induced upregulation in GLUT2 transcription (Fig. 4c, d). Similar findings were obtained in pGL3-GLUT2 and CB₁R-TK-d64 co-transfected cells exposed to HG in the presence of the mTORC1 inhibitor rapamycin (Fig. 4e). Interestingly, mTORC1 inhibition under normoglycemic conditions enhanced GLUT2 transcription (Fig. 4e). Taken together, these results strongly demonstrate that GLUT2 transcription under hyperglycemic conditions is regulated by a CB₁R/mTORC1 signaling pathway.

A few transcription factors (TFs) have been linked to regulating GLUT2 transcription in the proximal tubules^{65,66}; however, their regulation by CB₁R and mTORC1 has not yet been explored. We therefore unbiasedly screened a list of 46 potential candidate TFs (out of ~120) that were suggested by the TFBIND software to bind the hGLUT2 promoter (Supplementary Tables 3, 4). By using a promoter-binding transcription-factor profiling assay, we found that some of the TFs that were increased following the exposure of hRPTCs to HG were also competitively inhibited by adding hGLUT2 P1 promoter (Supplementary Fig. 7a, b). Of these, only



seven TFs (ATF6, STAT3, AP2, HNF4, CREB, HIF, and SREBP1) were profoundly altered (Fig. 4f), and their HG-induced activity was significantly inhibited by CB₁R or mTORC1 inhibition (Fig. 4g). However, when examining their mRNA expression levels in Akita-RPTC-CB₁R^{-/-} and Akita-RPTC-RPTOR^{-/-} diabetic mice, only SREBP1c was decreased in the absence of CB₁R or RPTOR (Fig. 4h, k), an effect that was translated to its protein

levels (Fig. 4i, j, l, m), and was found to be associated with the GLUT2 protein levels in these mice (Fig. 2c, f, j, l). Moreover, overactivation of mTORC1 in WT-RPTC-TSC^{-/-} mice resulted in enhanced expression of SREBP1 and GLUT2 (Supplementary Fig. 2g, h). To directly link SREBP1 with GLUT2 transcription, we knocked down SREBP1 in hRPTCs using siRNA, whose inhibition significantly reduced the GLUT2 expression levels under HG

Fig. 3 CB₁R modulates mTORC1 via a Gi-PI3K-dependent signaling pathway. **a–c** Representative immunoblots for pAKT and pS6 in primary hRPTCs treated with or without ACEA (10 μM), ACEA + JD5037 (100 nM) or ACEA + Wortmannin (500 nM) for 1 h. For **b**, $n = 3$ for Control group, $n = 4$ for ACEA and ACEA + JD5037 groups, $n = 5$ for ACEA + Wort group. For **c**, $n = 3$ for Control, ACEA and ACEA + JD5037 groups, $n = 5$ for ACEA + Wort group ($*P < 0.0116$, $#P < 0.0141$). **d–f** Representative immunoblots for pAKT and pS6 in primary hRPTCs treated with or without HG (30 mM), HG + JD5037 (100 nM) or HG + Wortmannin (500 nM) for 1 h. For **e**, $n = 15$ for Control group, $n = 16$ for HG group and $n = 12$ for HG + JD5037 and HG + Wort groups. For **f**, $n = 15$ for Control group, $n = 16$ for HG group and $n = 12$ for HG + JD5037 and HG + Wort groups ($*P < 0.0307$, $#P < 0.0003$). **g–i** Representative immunoblots for pAKT and pS6 in primary hRPTCs treated with or without ACEA (10 μM), ACEA + JD5037 (100 nM), ACEA + Pertussis toxin (100 ng/mL) or ACEA + YM254890 (1 μM) for 1 h. For **h**, $n = 4$ for Control, ACEA, ACEA + JD and ACEA + YM groups, $n = 5$ for ACEA + PTX group. For **i**, $n = 8$ per group ($*P < 0.0009$, $#P < 0.0025$). **j–l** Representative immunoblots for pAKT and pS6 in primary hRPTCs treated with or without HG (30 mM), HG + JD5037 (100 nM), HG + Pertussis toxin (100 ng/mL) or HG + YM254890 (1 μM) for 1 h. For **k**, $n = 9$ for Control, HG, HG + JD and HG + YM groups, $n = 8$ for ACEA + PTX group. For **l**, $n = 8$ per group ($*P < 0.0422$, $#P < 0.0020$). Data represent the mean ± SEM and were analyzed by One-way ANOVA followed by Tukey test (one-sided). $*P < 0.05$ relative to the corresponding control group. $#P < 0.05$ relative to the ACEA- or HG-treated group. Source data are provided as a Source Data file.

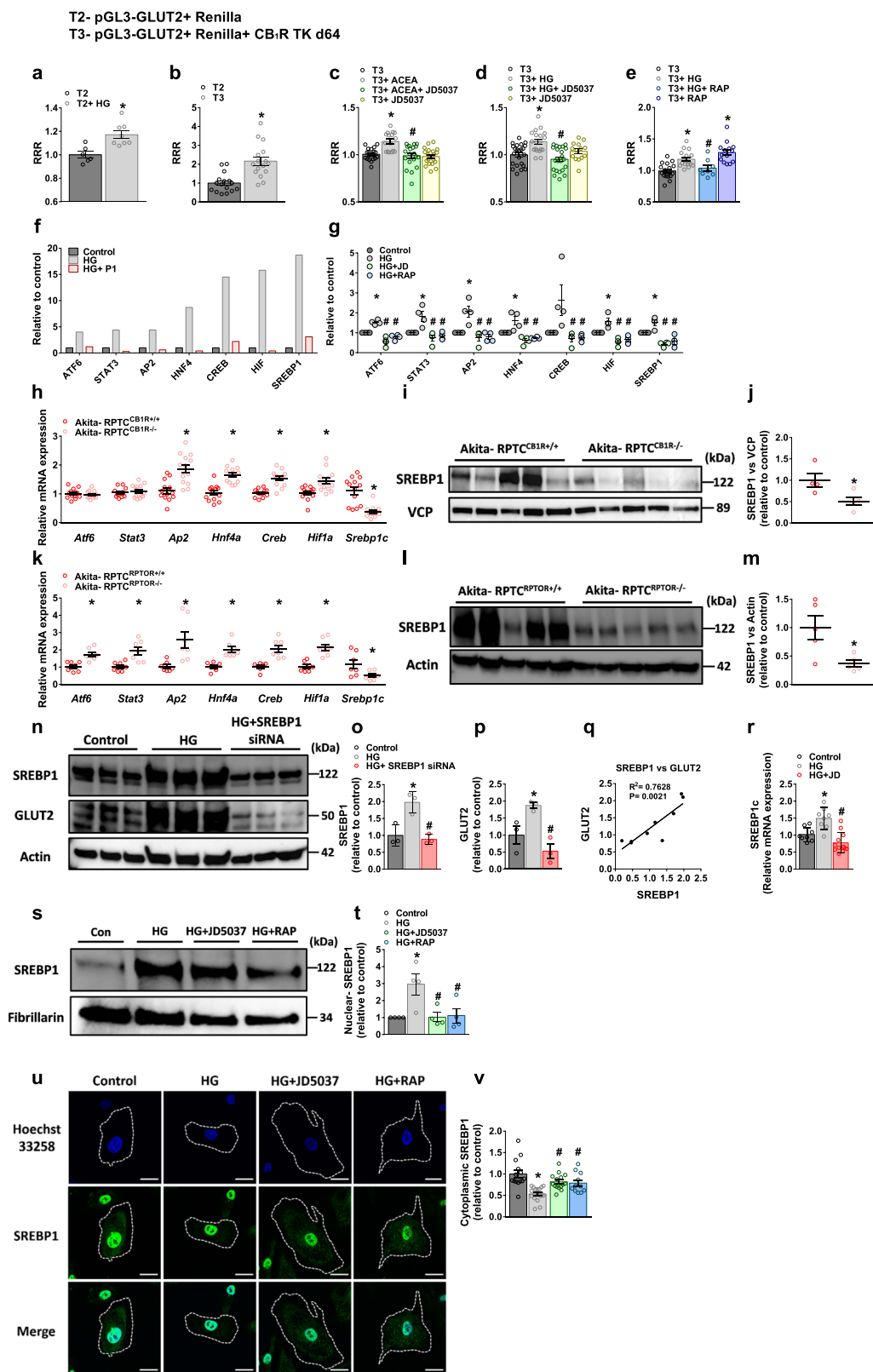
conditions, resulting in a positive correlation between the TF and its target protein (Fig. 4n–q). In addition, acute exposure of hRPTCs to HG conditions significantly elevated the gene expression levels of SREBP1c in a CB₁R-dependent manner (Fig. 4r), and enhanced its protein translocation from the cytoplasmic compartment to the nucleus, effects that were blocked by either JD5037 or rapamycin (Fig. 4s–v). Taken together, these results imply that activation of the CB₁R/mTORC1 signaling pathway under hyperglycemic conditions regulates GLUT2 transcription via SREBP1c.

CB₁R interacts with mTORC1 to maintain cellular homeostasis under normoglycemic conditions. To further assess the link between CB₁R and mTORC1 in RPTCs, we followed their association under normoglycemic conditions, and surprisingly, we noted the robust activation of mTORC1 in non-diabetic WT-RPTC-CB₁R^{-/-} mice, as manifested by the elevated pS6 and pAKT protein levels (Fig. 5a–d). This effect was accompanied by a significant elevation in the SREBP1 and GLUT2 protein expression levels (Fig. 5e–g), indicating a strong link between CB₁R and mTORC1 and their impact on GLUT2 transcription also during healthy conditions. Whereas reduced mTORC1 activity in normoglycemic WT-RPTC-RPTOR^{-/-} resulted in reduced SREBP1 expression, it did not yield a significant effect on the GLUT2 levels (Fig. 5h–k).

These surprising findings of an opposite regulation of mTORC1 by CB₁R in normal conditions led us to investigate the nutritional mediators (other than glucose) that may explain how CB₁R affects mTORC1 signaling. As it is already known, mTORC1 can be activated via signals coming from branched-chain amino acids (BCAAs) and protein degradation products⁶⁷. Indeed, CB₁R deletion in RPTCs resulted in an upregulation in the kidney mRNA and protein levels of megalin (LRP2) (Fig. 5l–o), a cellular membrane transporter responsible for the reuptake of lipoproteins, amino acids, vitamin-binding proteins, and hormones, as well as to a significant increase in the Na⁺-dependent neutral amino acid transporter B(0)AT1 (*SLC6A19*) (Fig. 5p, r, s) along with a marked upregulation in the expression of the large neutral amino acid transporter LAT1 (*SLC7A5*) (Fig. 5p, r, s). No significant changes were detected in the BCAA degrading enzymes (Fig. 5q). Interestingly, these changes were accompanied by elevated levels of kidney amino acids in WT-RPTC-CB₁R^{-/-} mice (Fig. 5t and Supplementary Table 7), which also persisted in the diabetic Akita-RPTC-CB₁R^{-/-} mice (Supplementary Fig. 8 and Supplementary Table 7), emphasizing the novel role of CB₁R in modulating amino acid uptake. *SLC6A19* amino acids transporter is Na⁺ dependent, and indeed we found decreased urinary levels of Na⁺ (Fig. 5u), implicating a higher Na⁺ utilization in the absence of CB₁R in RPTCs. Similarly, in hRPTCs under normoglycemic conditions, the CB₁R antagonist JD5037 upregulated the protein

levels of *SLC6A19* and *SLC7A5* (Supplementary Fig. 9a–c), further enhancing amino acid bioavailability to activate mTORC1 (Supplementary Fig. 9d, e). Moreover, CB₁R antagonism enhanced BCAAs uptake in hRPTCs (Supplementary Fig. 9f–i). The overactivation of kidney mTORC1 in WT-RPTC-CB₁R^{-/-} mice was accompanied by increased albuminuria and kidney injury (Fig. 6a–e), evident by abnormal morphological alterations, such as enlarged glomerular and Bowman's space cross sectional areas (Fig. 6f–i). Taken together, these findings indicate that under normal conditions RPTC CB₁R could restrain mTORC1 activity via regulating nutrient absorption to maintain normal kidney morphology and function.

Genetic reduction of GLUT2 in RPTCs protects mice from developing DKD. Following our finding that the CB₁R/mTORC1/SREBP1c signaling pathway regulates GLUT2 transcriptional expression in RPTCs, we next assessed whether a reduction in GLUT2 expression is sufficient to prevent DKD. To that end, we utilized the same breeding paradigm described earlier to generate diabetic mice lacking GLUT2 in RPTCs (Akita-RPTC-GLUT2^{-/-}) and their littermate control mice (Akita-RPTC-GLUT2^{+/+}) (Supplementary Fig. 10a–e). Whereas genetic reduction of GLUT2 specifically in RPTCs did not affect the susceptibility of the mice to develop insulin deficient diabetes (Fig. 7a–e), the null mice exhibited increased glycosuria (Fig. 7f) and preserved kidney function, manifested by reduced kidney-to-body weight ratio, urine excretion-to-water consumption ratio, as well as reduced proteinuria, albuminuria, urine creatinine, ACR, and urinary KIM-1 (Fig. 7g–m), without affecting BUN or CCr (Fig. 7n, o). Moreover, kidney morphological anomalies were prevented, including glomerular and Bowman's space areas hypertrophy and mesangial expansion (Fig. 7p–s). The expression of kidney injury, fibrosis, and inflammation markers was reduced in Akita-RPTC-GLUT2^{-/-} mice (Fig. 7t–v), suggesting that GLUT2 plays an obligatory role in the development of DKD. To further determine the role of RPTC-GLUT2 in glucose reabsorption by the kidney under diabetic conditions, we utilized an in vivo PET-MRI assay in which the GLUT high-affinity substrate, 2-deoxy-2-[¹⁸F]-fluoro-D-glucose (FDG), was injected into the tail vein and its uptake by different organs was analyzed. Kidney [¹⁸F]-FDG uptake was significantly increased in the diabetic mice (Fig. 7w–x), consequently increasing its concentration in the circulation and uptake in peripheral organs (e.g., the liver and muscle) while reducing its accumulation in the bladder (Supplementary Fig. 11a–h). Notably, these alterations were completely reversed in Akita-RPTC-GLUT2^{-/-} mice (Fig. 7w–x and Supplementary Fig. 11a–h), indicating the key role played by RPTC-GLUT2 in kidney glucose reabsorption. Interestingly, we found that deletion of GLUT2 in RPTCs significantly



downregulated SGLT2 expression under both normo- and hyperglycemic conditions in mice (Supplementary Fig. 12a–d). These findings may suggest that GLUT2 has a central role in modulating kidney glucose reabsorption and homeostasis by governing glucose transporters in the proximal tubules.

Discussion

The present study reveals, for the first time, the existence of a CB₁R/mTORC1 signaling axis in RPTCs and its importance in regulating kidney function in health and disease. Whereas CB₁R may restrain potentially deleterious mTORC1 over-activation

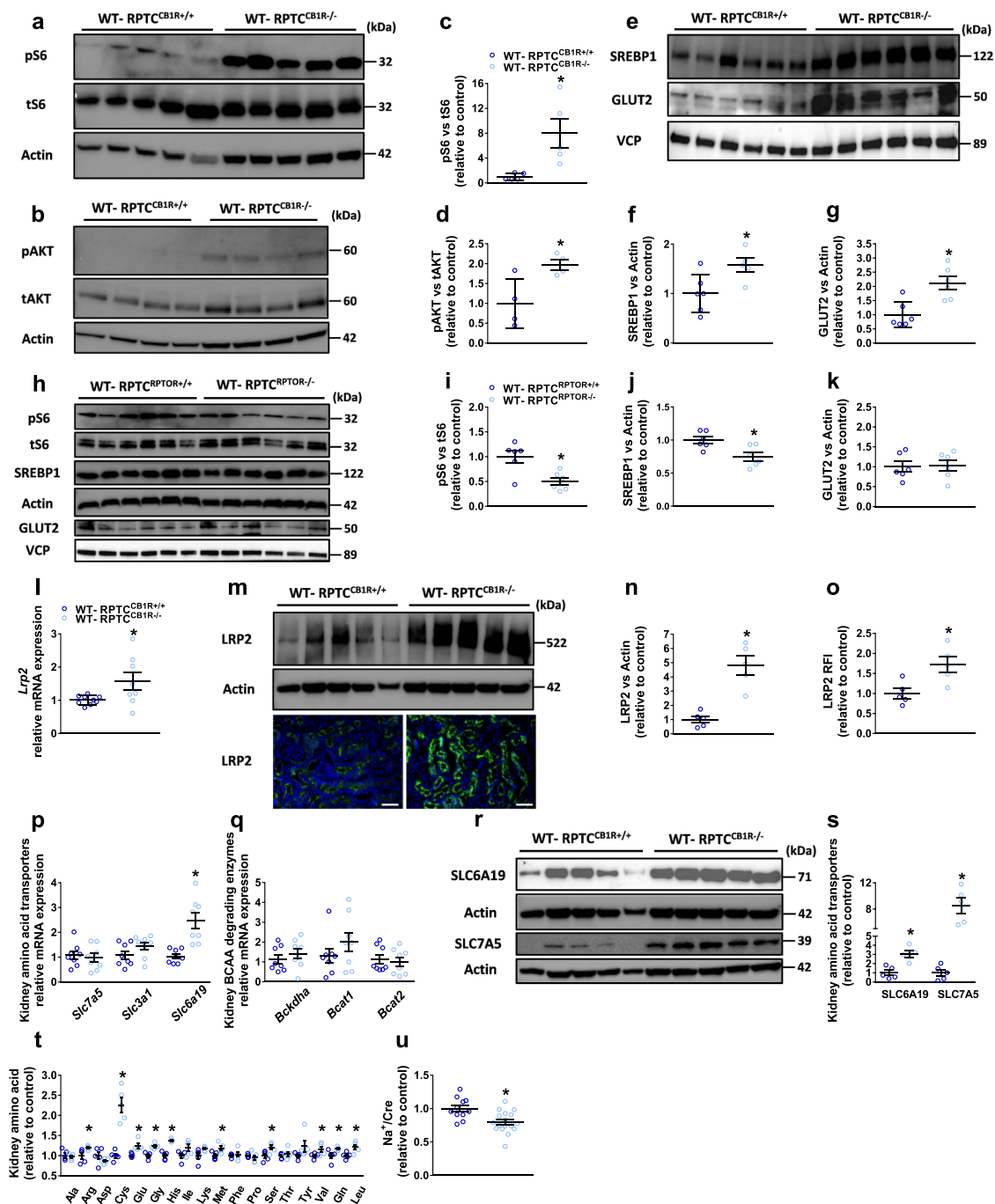
Fig. 4 GLUT2 transcription is directly regulated by CB₁R and mTORC1. **a–e** Luminescence relative response ratio (RRR) analyses of HEK293 cells co-transfected transiently with pGL3-GLUT and *Renilla* luciferase plasmids (T2) or with pGL3-GLUT, *Renilla* luciferase, and CB₁R-TK-d64 plasmids (T3), treated with or without ACEA (10 μM; **b, c**) or with HG (30 mM; **a, d, e**) for 3 h, in the presence or absence of JD5037 (100 nM) or rapamycin (100 nM). For **a**, $n = 6$ for T2, $n = 8$ for T2+HG ($*P = 0.0034$). For **b**, $n = 16$ per group ($*P < 0.0001$). For **c**, $n = 19$ for T3 group, $n = 16$ for T3 + ACEA group and $n = 20$ for T3 + ACEA + JD5037 and T3 + JD5037 groups ($*P < 0.0001$, $\#P = 0.0002$). For **d**, $n = 23$ for T3 and T3 + HG + JD5037 groups, $n = 19$ for T3 + HG group and $n = 14$ for T3 + JD5037 group ($*P = 0.0003$, $\#P = 0.0002$). For **e**, $n = 18$ for T3 group, $n = 16$ for T3 + HG group, $n = 8$ for T3 + HG + RAP group and $n = 14$ for T3 + RAP group ($*P < 0.0001$, $\#P = 0.0207$). **f** Promoter-binding transcription-factor (TF) profiling assay of the eight most prominent candidate TFs present in nuclear extracts (NEs) collected from primary hRPTCs treated with or without HG (30 mM) for 3 h in the presence or absence of hGLUT2 promoter (P1). **g** Transcription-factor profiling assay for eight candidate TFs present at the NEs of primary hRPTCs treated with or without HG (30 mM) in the presence or absence of JD5037 (100 nM) or rapamycin (100 nM) for 3 h. $n = 4$ per group ($*P < 0.0019$, $\#P < 0.0001$). **h** qPCR analyses of kidney *Glut2* candidate TFs in kidney lysate from Akita-RPTC^{CB1R+/+} and Akita-RPTC^{CB1R-/-} diabetic mice. $n = 13$ mice per group ($*P < 0.0018$). **i, j** Immunoblotting analysis and quantification of SREBP1 in kidney lysate from Akita-RPTC^{CB1R+/+} and Akita-RPTC^{CB1R-/-} diabetic mice. $n = 4$ mice for Akita-RPTC^{CB1R+/+}, $n = 5$ mice for Akita-RPTC^{CB1R-/-} ($*P = 0.0264$). **k** qPCR analysis and quantification of kidney *Glut2* candidate TFs in kidney lysate from Akita-RPTC^{RPTOR+/+} and Akita-RPTC^{RPTOR-/-} diabetic mice. $n = 7$ mice per group ($*P < 0.0324$). **l, m** Immunoblotting analysis and quantification of SREBP1 in kidney lysate from Akita-RPTC^{RPTOR+/+} and Akita-RPTC^{RPTOR-/-} diabetic mice. $n = 5$ mice per group ($*P = 0.0191$). **n–q** Immunoblotting analysis of SREBP1c and GLUT2 in primary hRPTCs treated with or without HG (30 mM) in the presence or absence of SREBP1 siRNA for 24 h. $n = 3$ biological replicates per group ($*P < 0.0385$, $\#P < 0.0051$). **r** qPCR analysis of SREBP1c in primary hRPTCs treated with or without HG (30 mM) in the presence or absence of JD5037 (100 nM) for 1 h. $n = 8$ for Control and HG groups, $n = 12$ for HG + JD group ($*P = 0.0031$, $\#P < 0.0001$). **s, t** Representative immunoblotting analysis and quantification of nuclear SREBP1 in extracts collected from primary hRPTCs treated with or without HG (30 mM) in the presence or absence of JD5037 (100 nM) or rapamycin (100 nM) for 3 h. SREBP1 expression was normalized to the nuclear marker Fibrillarin. $n = 4$ per group ($*P = 0.0196$, $\#P < 0.0497$). **u, v** Representative immunofluorescence and quantification of cytoplasmic SREBP1 expression in primary hRPTCs treated with or without HG (30 mM) in the presence or absence of JD5037 (100 nM) or rapamycin (100 nM) for 3 h. 100× magnification, scale bar: 10 μm. $n = 14$ for Control group, $n = 19$ for HG group, $n = 15$ for HG + JD5037 group and $n = 11$ for HG + RAP group ($*P < 0.0001$, $\#P < 0.0012$). Data represent the mean ± SEM and were analyzed by unpaired two-tailed Student's t-test or one-way ANOVA followed by Tukey test (one-sided). $*P < 0.05$ relative to the corresponding control group. $\#P < 0.05$ relative to the ACEA- or HG-treated group. Source data are provided as a Source Data file.

during normoglycemia by preventing amino acid flux, in diabetes, enhanced activity of CB₁R by eCBs, stimulates mTORC1 to further increase glucose uptake via upregulating SREBP1-mediated GLUT2 expression, thus contributing to the development of DKD (Fig. 8). These novel findings have developmental, functional, and translational implications.

Under normoglycemic physiological condition, kidney CB₁R regulates hemodynamic by inducing afferent arterioles vasodilation and reducing GFR^{68,69}. CB₁R has been suggested to regulate Na⁺/K⁺-ATPase activity in RPTCs^{63,70}, which is required for maintaining the electrochemical sodium gradient across the brush border membrane of the RPTCs, and it is therefore essential for the reabsorption process that occurs in the kidney. Similar to CB₁R, mTORC1 also plays an essential physiological role in regulating nutrient transport in RPTCs⁷¹. Mice lacking mTORC1 in RPTCs⁷¹ or treated with rapamycin develop glycosuria, phosphaturia, aminoaciduria, low-molecular weight proteinuria, and albuminuria⁷², findings observed in individuals suffering from the Fanconi-Bickel syndrome, caused by mutations in the *GLUT2* gene, *SLC2A2*^{73,74}. Interestingly, we found that deletion of CB₁R from RPTCs in non-diabetic animals stimulated mTORC1 signaling resulting in kidney dysfunction. This effect was associated with increased amino acid content and bioavailability in RPTC-CB₁R^{-/-} mice and hRPTCs treated with a CB₁R antagonist. Increased BCAA content in the kidney of these animals and cells is most likely mediated via megalin and the neutral amino acid transporter SLC6A19 as well as the large neutral amino acid transporter, SLC7A5. CB₁R has been previously shown to regulate kidney megalin expression in diet-induced obesity^{75,76}. SLC6A19 was also suggested as a potential target for the treatment of metabolic disorders, since its absence in mice was associated with decreased mTORC1 activity^{77,78}. In fact, the absence of CB₁R may alter Na⁺/K⁺-ATPase^{63,70}, required for SLC6A19 activity. SLC7A5, known to be expressed in proximal tubular cells⁷⁹, was shown to activate mTORC1 via transporting Leucine into the lysosome⁸⁰. We show here that these transporters are regulated by CB₁R. Although Cystine levels were highly upregulated in mice lacking CB₁R, no changes were detected in the levels of the Cystine transporter SLC3A1. Grahammer and

colleagues showed that genetic depletion of mTORC1 in the proximal tubules decreased the expression and/or phosphorylation of multiple amino acid transporters, leading to aminoaciduria⁷¹, emphasizing a direct role for mTORC1 in amino acid transport. We have previously reported that genetic manipulations of mTORC1 in RPTCs, both constant activation, and inhibition by TSC1 KO and RPTOR KO respectively, modulate SLC6A19 expression⁵⁸. Therefore, we cannot exclude the possibility that prolonged mTORC1 activation in RPTC-CB₁R^{-/-} mice per se lead to enhanced amino acid transport. Nevertheless, megalin and cubilin expression was unchanged in mTORC1-depleted tubules⁷¹; therefore, the specific role of CB₁R in modulating mTORC1 activity via megalin/cubilin mediated amino acids transport cannot be negated. Moreover, we previously reported that genetic deletion of CB₁R in RPTCs increases kidney weight and glomerular area²¹, implying that CB₁R may play a developmental role in the kidney. The present study offers an explanation for this phenomenon through a hitherto unrecognized CB₁R-mediated regulation of mTORC1, known to control cell metabolism, growth, and proliferation. Thus, our current findings raise a concern for using CB₁R antagonists in normoglycemic patients because they may enhance mTORC1 activity and induce deleterious effects on the kidney.

Whereas under normoglycemic conditions CB₁R controls mTORC1 activation in RPTCs via restraining amino acids flux, our findings demonstrate that glucotoxicity enhances CB₁R-induced mTORC1 activity in the same type of cells. In accordance with previous findings with CB₁R blockers^{17,19,25}, specific deletion of RPTC-CB₁R in *Akita* diabetic mice, although not affecting the diabetic phenotype of the animals, had a profound beneficial effect on the kidney, which can be attributed to the inhibition of mTORC1 signaling. These findings were associated with reduced GLUT2 expression and glucosuria, effects that were previously described by us as being modulated by kidney CB₁R²⁵. In agreement with our findings, it was recently demonstrated that pancreatic GLUT2 levels are reduced in CB₁R/CB₂R-deficient mice⁸¹. Mechanistically, our findings show here that CB₁R regulates mTORC1 in RPTCs via the PI3K-Akt pathway under diabetic



conditions. Dalton and colleagues suggested that the $\beta\gamma$ subunits of the CB_1R -coupled $G_{i/o}$ protein in neuronal cells stimulate PI3K to induce ERK phosphorylation⁵⁹. On the contrary, we found that stimulation of CB_1R by glucose did not affect (or even reduced) the phosphorylation of ERK in RPTCs and that mTORC1 activation is mediated via a $G_{i/o}$ protein coupled CB_1R pathway. We and others^{82,83} have previously shown that CB_1R may also signal via G_q signaling, which enhances cellular calcium influx, contributing to increased PKC- β 1 expression, resulting in dynamic translocation of GLUT2 into the brush border membrane of the RPTCs²⁵. Such a duality in the cellular signaling cascades modulated by CB_1R can exist in RPTCs⁶³, allowing CB_1R to modulate both the expression and the translocation of GLUT2. Alternatively, CB_1R activation can stimulate phospholipase C (PLC) via the $G_{i/o}$ $\beta\gamma$ subunit, thereby increasing intracellular $[Ca^{2+}]$ influx and PKC

activation⁶¹. Consistently, we found (i) significant positive correlation between pS6 and pAKT and GLUT2, (ii) modulation of GLUT2 expression in mice lacking RPTOR or TSC1 specifically in RPTCs, and (iii) increased transcriptional expression of GLUT2 by HG and/or CB_1R activation, effects that were completely prevented by CB_1R or mTORC1 inhibition.

As per the transcriptional regulation of GLUT2 in RPTCs^{65,66}, we found 24 TFs that were enriched in the nuclear compartment of hRPTCs exposed to HG and that selectively bind to the GLUT2 promoter. The most prominent one, SREBP1c, has been previously shown to promote kidney lipotoxicity^{84–87}. It has been also reported that in RPTCs, hepatocytes, and Schwann cells, HG stimulates SREBP1c via the PI3K/AKT/mTORC1 pathway^{42,87–90}. Moreover, SREBP1c enhances GLUT2 expression in hepatocytes exposed to

Fig. 5 CB₁R regulates mTORC1 activation under normoglycemic conditions. **a, c** Immunoblotting analysis and quantification of pS6 in kidney lysates from WT-RPTC^{CB1R+/+} and WT-RPTC^{CB1R-/-} normoglycemic mice. $n = 5$ mice per group ($*P = 0.0166$). **b, d** Immunoblotting analysis and quantification of pAKT in kidney lysates from WT-RPTC^{CB1R+/+} and WT-RPTC^{CB1R-/-} normoglycemic mice. $n = 4$ mice per group ($*P = 0.0275$). **e-g** Immunoblotting analysis and quantification of SREBP1c and GLUT2 in kidney lysates from WT-RPTC^{CB1R+/+} and WT-RPTC^{CB1R-/-} normoglycemic mice. $n = 6$ mice per group ($*P < 0.0264$). **h-k** Immunoblotting analysis and quantification of pS6, SREBP1c, and GLUT2 in kidney lysates from WT-RPTC^{RPTOR+/+} and WT-RPTC^{RPTOR-/-} normoglycemic mice. $n = 6$ mice per group ($*P < 0.0136$). **l** qPCR analyses of megalin (*Lrp2*) in kidney lysates from WT-RPTC^{CB1R+/+} and WT-RPTC^{CB1R-/-} normoglycemic mice. $n = 9$ mice for WT-RPTC^{CB1R+/+}, $n = 8$ mice for WT-RPTC^{CB1R-/-} ($*P = 0.0395$). **m** Representative LRP2 immunoblotting and immunofluorescence staining of kidney sections from WT-RPTC^{CB1R+/+} and WT-RPTC^{CB1R-/-} normoglycemic mice. 10 \times magnification, scale bar 100 μ m. $n = 5$ mice per group. **n** Immunoblotting quantification of LRP2 in kidney lysates from WT-RPTC^{CB1R+/+} and WT-RPTC^{CB1R-/-} normoglycemic mice. $n = 5$ mice per group ($*P = 0.0007$). **o** Immunofluorescence quantification for LRP2 in kidney sections from WT-RPTC^{CB1R+/+} and WT-RPTC^{CB1R-/-} normoglycemic mice. 10 \times magnification, scale bar 100 μ m. $n = 5$ mice per group ($*P = 0.0164$). **p** qPCR analysis of amino acid transporters in kidney lysates from WT-RPTC^{CB1R+/+} and WT-RPTC^{CB1R-/-} normoglycemic mice. $n = 8$ mice per group ($*P = 0.0007$). **q** qPCR analysis of BCAA degrading enzymes in kidney lysates from WT-RPTC^{CB1R+/+} and WT-RPTC^{CB1R-/-} normoglycemic mice. $n = 8$ mice per group. **r, s** Immunoblotting analysis and quantification of SLC6A19 and SLC7A5 in kidney lysates from WT-RPTC^{CB1R+/+} and WT-RPTC^{CB1R-/-} normoglycemic mice. $n = 5$ mice per group ($*P < 0.0017$). **t** LC-MS/MS quantification of amino acids in kidney lysates from WT-RPTC^{CB1R+/+} and WT-RPTC^{CB1R-/-} normoglycemic mice. $n = 5$ mice per group ($*P < 0.0354$). **u** Urinary Na⁺ levels normalized to the creatinine concentration. $n = 11$ mice for WT-RPTC^{CB1R+/+}, $n = 17$ mice for WT-RPTC^{CB1R-/-} ($*P = 0.0031$). Data represent the mean \pm SEM and were analyzed by unpaired two-tailed Student's t-test. $*P < 0.05$ relative to the corresponding control groups. Source data are provided as a Source Data file.

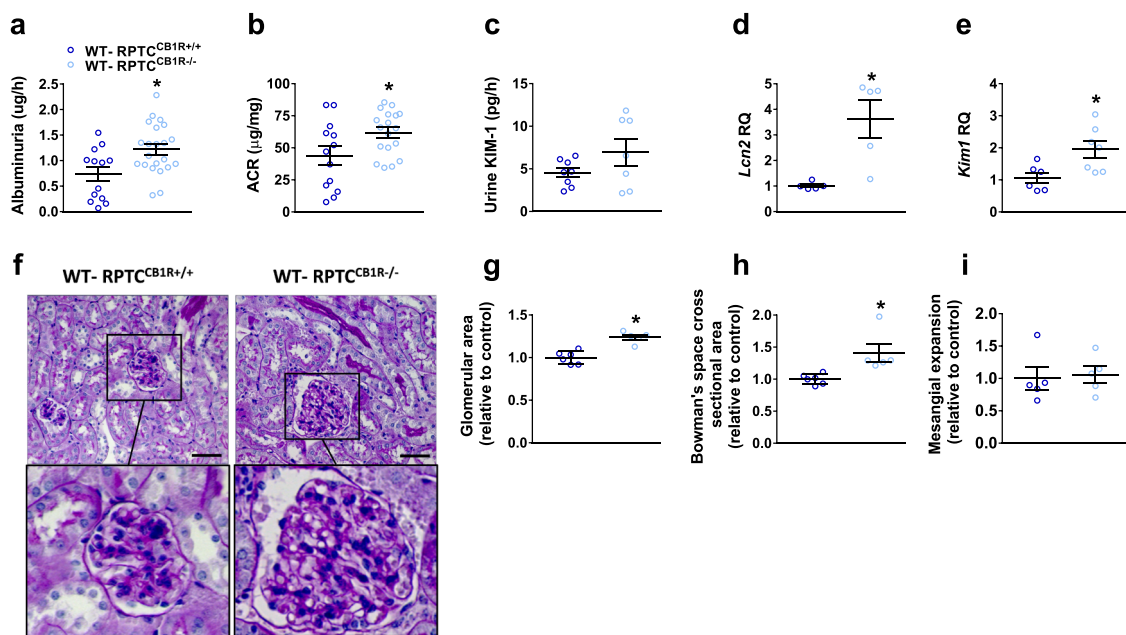
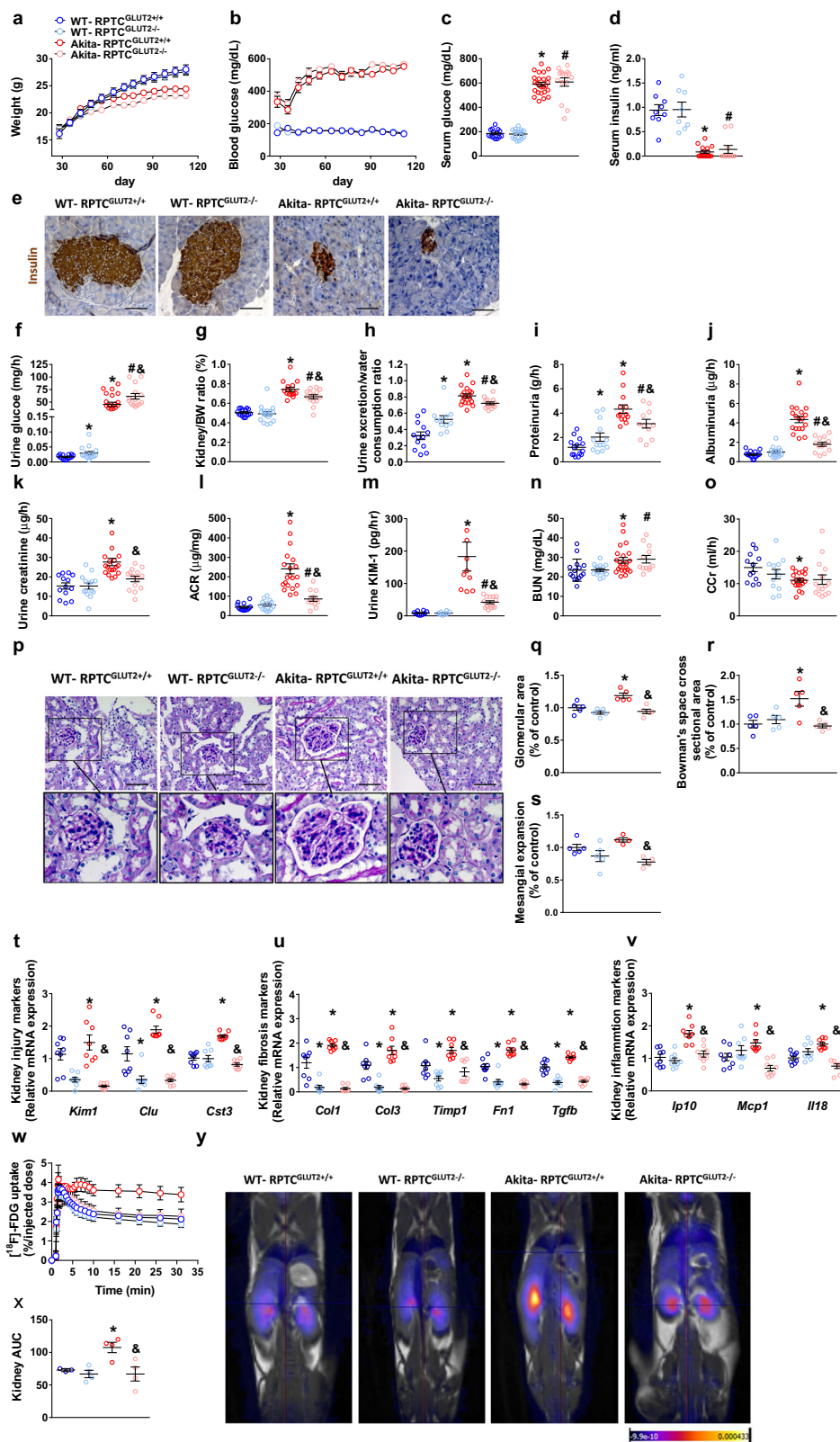


Fig. 6 mTORC1 overactivation in RPTC-CB₁R KO mice promotes kidney functional and morphological abnormalities. **a** Albuminuria in 16-week-old normoglycemic mice. $n = 13$ mice for WT-RPTC^{CB1R+/+}, $n = 22$ mice for WT-RPTC^{CB1R-/-} ($*P = 0.0079$). **b** Urine albumin-to-creatinine ratio (ACR) in 16-week-old normoglycemic mice. $n = 13$ mice for WT-RPTC^{CB1R+/+}, $n = 18$ mice for WT-RPTC^{CB1R-/-} ($*P = 0.0301$). **c** Urinary KIM-1 levels in 16-week-old normoglycemic mice. $n = 8$ mice for WT-RPTC^{CB1R+/+}, $n = 7$ mice for WT-RPTC^{CB1R-/-}. **d** qPCR analysis of the kidney injury marker, *Lcn2*. $n = 5$ mice per group ($*P = 0.0070$). **e** qPCR analysis of the kidney injury marker, *Kim1*. $n = 6$ mice for WT-RPTC^{CB1R+/+}, $n = 7$ mice for WT-RPTC^{CB1R-/-} ($*P = 0.0197$). **f** Representative PAS staining of the kidney, 40 \times magnification, scale bar: 50 μ m. **g** Glomerular area quantification (at least 10 glomeruli per mouse). $n = 6$ mice for WT-RPTC^{CB1R+/+}, $n = 5$ mice for WT-RPTC^{CB1R-/-} ($*P = 0.0004$). **h** Bowman's space cross-sectional area quantification (at least 10 glomeruli per mouse). $n = 6$ mice for WT-RPTC^{CB1R+/+}, $n = 5$ mice for WT-RPTC^{CB1R-/-} ($*P = 0.0142$). **i** Mesangial expansion quantification (at least 10 glomeruli per mouse). $n = 6$ mice for WT-RPTC^{CB1R+/+}, $n = 5$ mice for WT-RPTC^{CB1R-/-}. Data represent the mean \pm SEM and were analyzed by Unpaired Two-tailed Student's t-test. $*P < 0.05$ relative to the corresponding control groups. Source data are provided as a Source Data file.

hyperglycemia⁹¹. In line with the recent reports, we also found that specific genetic deletion of CB₁R, RPTOR, or TSC1 in the RPTCs modulated SREBP1c levels in parallel to GLUT2 expression. Furthermore, treatment of hRPTCs with rapamycin stimulated GLUT2 transcriptional activity. Collectively, these findings demonstrate the importance of SREBP1c in modulating the CB₁R/mTORC1 effect on GLUT2.

Here, we also demonstrate a direct effect of glucose on the production and/or degradation of 2-AG, which in turn, may

activate its own receptor to further promote glucose transport resulting in RPTC's dysfunction. These findings are in line with previous reports showing increased eCB/CB₁R 'tone' in different compartments/cells within the kidney as well as in pancreatic islets under gluco- and/or lipo-toxic conditions^{17,20,21,92}. As previously reported by Sampaio and colleagues, the two isoforms of DAGL are differentially expressed in the renal proximal tubule⁶³. While we did not find any changes in their expression in response to hyperglycemia, the functional inhibition of DAGL



resulted in reduced GLUT2 levels in hRPTCs, suggesting that increased 2-AG levels by glucose are mediated via DAGL.

Global GLUT2^{-/-} mice display severe glycosuria⁹³, and the complete absence of GLUT2 at the basolateral membrane of the RPTCs supposedly leads to enhanced intracellular glucose levels

and proximal tubular damage, even in the absence of diabetes. This effect has been well-documented in Fanconi-Bickel Syndrome patients who exhibit tubular dysfunction⁹⁴. However, our current study revealed additional surprising phenomena. Specific reduction, but not full ablation of GLUT2 in RPTCs ameliorates

Fig. 7 Genetic reduction of GLUT2 in RPTCs protects mice from developing DKD. All the following measurements were done in Akita diabetic mice and their littermate WT controls with or without reduced expression of GLUT2 in RPTCs: **a** Body weight surveillance for a period of 16 weeks. $n = 16$ mice for WT-RPTC^{GLUT2+/+}, $n = 17$ mice for WT-RPTC^{GLUT2-/-}, $n = 20$ mice for Akita-RPTC^{GLUT2+/+}, $n = 17$ mice for Akita-RPTC^{GLUT2-/-}. **b** Blood glucose surveillance for a period of 16 weeks. $n = 16$ mice for WT-RPTC^{GLUT2+/+}, $n = 17$ mice for WT-RPTC^{GLUT2-/-}, $n = 20$ mice for Akita-RPTC^{GLUT2+/+}, $n = 17$ mice for Akita-RPTC^{GLUT2-/-}. **c** Serum glucose. $n = 16$ mice for WT-RPTC^{GLUT2+/+}, $n = 17$ mice for WT-RPTC^{GLUT2-/-}, $n = 20$ mice for Akita-RPTC^{GLUT2+/+}, $n = 17$ mice for Akita-RPTC^{GLUT2-/-} ($*P < 0.0062$, $\#P = 0.0002$, $\&P = 0.0082$). **d** Serum insulin. $n = 9$ mice for WT-RPTC^{GLUT2+/+}, $n = 8$ mice for WT-RPTC^{GLUT2-/-}, $n = 15$ mice for Akita-RPTC^{GLUT2+/+}, $n = 10$ mice for Akita-RPTC^{GLUT2-/-} ($*P < 0.0437$, $\#P = 0.0001$). **e** Representative insulin immunohistochemistry staining in the pancreas, 40 \times magnification, scale bar: 50 μ m. **f** Urinary glucose levels. $n = 16$ mice for WT-RPTC^{GLUT2+/+}, $n = 17$ mice for WT-RPTC^{GLUT2-/-}, $n = 20$ mice for Akita-RPTC^{GLUT2+/+}, $n = 17$ mice for Akita-RPTC^{GLUT2-/-} ($*P < 0.0062$, $\#P < 0.0001$, $\&P = 0.0288$). **g** Kidney-to-body weight ratio. $n = 16$ mice for WT-RPTC^{GLUT2+/+}, $n = 17$ mice for WT-RPTC^{GLUT2-/-}, $n = 20$ mice for Akita-RPTC^{GLUT2+/+}, $n = 17$ mice for Akita-RPTC^{GLUT2-/-} ($*P < 0.0001$, $\#P < 0.0001$, $\&P = 0.0187$). **h** Urine exertion-to-water consumption ratio. $n = 16$ mice for WT-RPTC^{GLUT2+/+}, $n = 17$ mice for WT-RPTC^{GLUT2-/-}, $n = 20$ mice for Akita-RPTC^{GLUT2+/+}, $n = 17$ mice for Akita-RPTC^{GLUT2-/-} ($*P < 0.0062$, $\#P = 0.0002$, $\&P = 0.0082$). **i** Urinary protein levels. $n = 14$ mice for WT-RPTC^{GLUT2+/+}, $n = 13$ mice for WT-RPTC^{GLUT2-/-} and Akita-RPTC^{GLUT2+/+}, $n = 11$ mice for Akita-RPTC^{GLUT2-/-} ($*P < 0.0418$, $\#P = 0.0389$, $\&P = 0.0282$). **j** Urinary albumin levels. $n = 15$ mice for WT-RPTC^{GLUT2+/+}, $n = 15$ mice for WT-RPTC^{GLUT2-/-}, $n = 18$ mice for Akita-RPTC^{GLUT2+/+}, $n = 13$ mice for Akita-RPTC^{GLUT2-/-} ($*P < 0.0001$, $\#P = 0.0030$, $\&P < 0.0001$). **k** Urinary creatinine levels. $n = 13$ mice for WT-RPTC^{GLUT2+/+}, $n = 14$ mice for WT-RPTC^{GLUT2-/-}, $n = 20$ mice for Akita-RPTC^{GLUT2+/+}, and $n = 14$ mice for Akita-RPTC^{GLUT2-/-} ($*P < 0.0001$, $\&P = 0.0019$). **l** Urine albumin-to-creatinine ratio (ACR). $n = 14$ mice for WT-RPTC^{GLUT2+/+}, $n = 14$ mice for WT-RPTC^{GLUT2-/-}, $n = 20$ mice for Akita-RPTC^{GLUT2+/+}, and $n = 12$ mice for Akita-RPTC^{GLUT2-/-} ($*P < 0.0001$, $\#P = 0.0326$, $\&P = 0.0001$). **m** Urinary KIM-1 levels. $n = 10$ mice for WT-RPTC^{GLUT2+/+}, $n = 8$ mice for WT-RPTC^{GLUT2-/-}, $n = 10$ mice for Akita-RPTC^{GLUT2+/+}, and $n = 14$ mice for Akita-RPTC^{GLUT2-/-} ($*P = 0.0010$, $\#P < 0.0001$, $\&P = 0.0011$). **n** Urinary BUN. $n = 15$ mice for WT-RPTC^{GLUT2+/+}, $n = 15$ mice for WT-RPTC^{GLUT2-/-}, $n = 22$ mice for Akita-RPTC^{GLUT2+/+} and $n = 12$ mice for Akita-RPTC^{GLUT2-/-} ($*P = 0.0261$, $\#P = 0.0076$). **o** Creatinine clearance (CCr). $n = 12$ mice for WT-RPTC^{GLUT2+/+}, $n = 12$ mice for WT-RPTC^{GLUT2-/-}, $n = 20$ mice for Akita-RPTC^{GLUT2+/+}, and $n = 15$ mice for Akita-RPTC^{GLUT2-/-} ($*P = 0.0034$). **p** Representative PAS staining of the kidney, 40 \times magnification, scale bar: 50 μ m. **q** Glomerular area quantification (at least 10 glomeruli per mouse). $n = 5$ mice per group ($*P = 0.0096$, $\&P = 0.0015$). **r** Bowman's space cross-sectional area quantification (at least 10 glomeruli per mouse). $n = 5$ mice per group ($*P = 0.0160$, $\&P = 0.0075$). **s** Mesangial expansion quantification (at least 10 glomeruli per mouse). $n = 5$ mice for WT-RPTC^{GLUT2+/+} and WT-RPTC^{GLUT2-/-}, $n = 4$ mice for Akita-RPTC^{GLUT2+/+} and Akita-RPTC^{GLUT2-/-} ($\&P = 0.0006$). **t** qPCR analysis of kidney injury markers *Kim1*, *Clu*, and *Cst3*. $n = 8$ mice per group ($*P < 0.0091$, $\&P < 0.0001$). **u** qPCR analysis of kidney fibrogenic markers *Col1*, *Col3*, *Timp1*, *Fn1*, and *Tgfb*. $n = 8$ mice per group ($*P < 0.0173$, $\&P < 0.0008$). **v** qPCR analyses of kidney inflammatory markers *Ip10*, *Mcp1*, and *Il18*. $n = 8$ mice per group ($*P < 0.0122$, $\&P < 0.0006$). **w, x** Kidney uptake of [¹⁸F]-FDG using PET-MRI analysis. $n = 3$ mice for WT-RPTC^{GLUT2+/+}, $n = 4$ mice for WT-RPTC^{GLUT2-/-}, Akita-RPTC^{GLUT2+/+} and Akita-RPTC^{GLUT2-/-} ($*P = 0.0139$, $\&P = 0.0224$). **y** Representative kidneys PET-MRI images. Data represent the mean \pm SEM and were analyzed by one-way ANOVA followed by Tukey test (one-sided). $*P < 0.05$ relative to the WT-RPTC^{GLUT2+/+} mice; $\#P < 0.05$ relative to WT-RPTC^{GLUT2-/-} mice; $\&P < 0.05$ relative to the Akita-RPTC^{GLUT2+/+} mice. Source data are provided as a Source Data file.

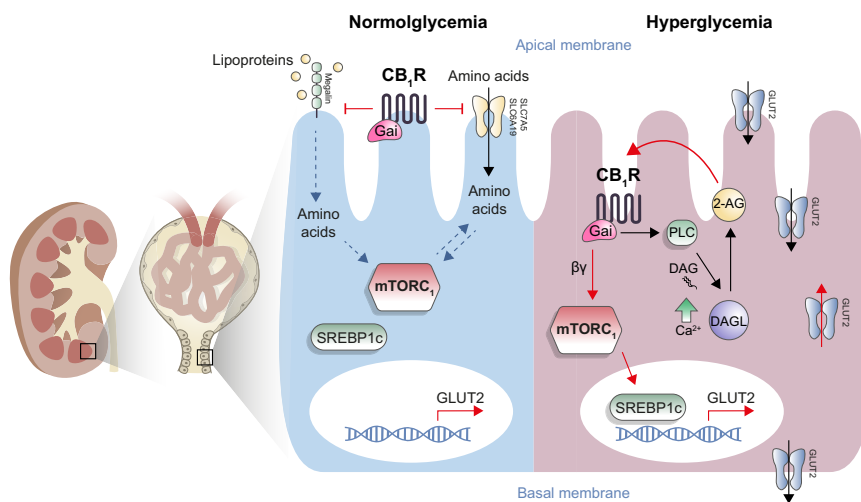


Fig. 8 A proposed mechanism by which renal proximal tubule CB₁R regulates mTORC1 activity in health and disease. In normoglycemia CB₁R is responsible to maintain mTORC1 normal activation by preventing excess of amino acids uptake (left). In hyperglycemia, CB₁R-mediated mTORC1 overactivation results in upregulating GLUT2 transcription, consequently enhancing glucose absorption and tubular damage (right).

the development of DKD in Akita-RPTC-GLUT2^{-/-} mice. Proximal tubular GLUT2 is known to be upregulated and translocated to the brush border membrane of the RPTCs where it facilitates glucose reabsorption during diabetes^{55,95}, and may increase glucose-induced tubular damage and tubule-interstitial fibrosis. The contribution of GLUT2 recruitment to the brush border membrane of the RPTCs in facilitating increased glucose reabsorption in diabetes is not clear, since kidney glucose

reabsorption is also mediated via SGLT2 and SGLT1⁹⁶. Possibly, in diabetes, luminal glucose concentrations exceed a point by which SGLT's glucose uptake is in its full capacity, GLUT2 recruitment to the apical membrane enables glucose "leakiness" back to the lumen, facilitating apical glucose recycling to promote sodium reabsorption through SGLTs⁶. Moreover, rising blood glucose levels hamper the tubule-to-blood glucose gradient, which is essential for glucose flux through basolateral GLUT2⁹⁷.

Therefore, to maintain ‘normal’ tubular glucose levels, GLUT2 is recruited to the apical brush border membrane to assist in glucose transfer into the cell. Marks and colleagues found that STZ-induced diabetes in rats increases facilitative glucose transport at the brush border membrane by 67.5%, mainly due to GLUT2 translocation⁵⁵. Our novel *in vivo* PET-MRI data emphasize the key role of GLUT2 in glucose reabsorption in diabetes, since its ablation in RPTCs normalized the diabetes-induced glucose uptake to the kidney. In addition, Umino et al. suggested that activation of the GLUT2/importin- α 1/HNF-1 α pathway by basolateral HG enhances SGLT2 expression in RPTCs; this was preventable by GLUT2 silencing/inhibition⁹⁸. These findings are also supported by our data, demonstrating that genetic deletion of GLUT2 in RPTCs decreased SGLT2 expression, regardless the status of glycemia, suggesting that tight crosstalk between these two glucose transporters regulates kidney glucose handling and function.

Our results may also have translational aspects when one considers the therapeutic potential of pharmacologically targeting GLUT2 for the treatment of DKD. However, GLUT2 inhibition is unlikely to discriminate between apical and basal GLUT2 and might have major systemic side-effects as GLUT2 plays a role in glucose transport in other tissues, including the gut, islets, the liver, and neurons. Moreover, kidney glucose toxicity may remain an issue if glucose is taken up into RPTCs via SGLT2 but cannot exit to the interstitium and the blood at the basolateral side. Therefore, from this perspective, targeting the CB₁R and its downstream signaling molecules identified here may be a more fruitful therapeutic strategy. An alternative approach would be to target the recruitment machinery of GLUT2 to the brush border membrane to restrain the development of DKD rather than targeting the transporter itself. Further work is required to test which option might become a vital therapeutic approach for DKD.

Methods

Animals and the experimental protocol. The Institutional Animal Care and Use Committee of the Hebrew University (AAALAC accreditation #1285; Ethic approval number MD-19-15784) approved the experimental protocol used. Animal studies are reported, in compliance with the ARRIVE guidelines⁹⁹. The current experiment is based on the rule of the replacement, refinement, or reduction. All the animals used in this study were males under C57BL/6J background that were housed under specific pathogen-free (SPF) conditions, up to five per cage, in standard plastic cages with natural soft sawdust as bedding. The animals were maintained under controlled temperature of 22–24 °C, humidity at 55 ± 5%, and alternating 12 h light/dark cycles (lights were on between 7:00 and 19:00 h), and provided with chow food (Cat#, NIH-31 rodent diet) and water *ad libitum*. To elucidate the role of the proximal tubular CB₁R in the pathogenesis of DKD, we generated a novel diabetic mouse strain that lacks CB₁R specifically in the RPTCs (AK-RPTC-CB₁R^{-/-}) by crossing the Akita^{Ins2+/C96Y} mouse model for type I diabetes with RPTC-CB₁R^{fl/fl;sglt2Cre} [RPTC-CB₁R^{-/-}] characterized previously^{21,25}. To generate diabetic mice lacking GLUT2 in RPTCs, we first crossed mice containing two *loxP* sites flanking the open reading frame of the GLUT2 gene (GLUT2^{fl/fl}, described in¹⁰⁰) with the *iL1-sglt2-Cre* line¹⁰¹. Then RPTC-GLUT2^{fl/fl;sglt2Cre} (RPTC-GLUT2^{-/-}) were crossed with Akita^{Ins2+/C96Y} to generate AK-RPTC-GLUT2^{-/-} mice. To generate diabetic mice lacking RPTOR in RPTCs, we first crossed mice containing two *loxP* sites flanking the open reading frame of the RPTOR gene (*Raptor*^{fl/fl}, #013188, Jackson Laboratories, Bar Harbor, ME) with the *iL1-sglt2-Cre* line¹⁰¹. Then, RPTC-RPTOR^{fl/fl;sglt2Cre} (RPTC-RPTOR^{-/-}) were crossed with Akita^{Ins2+/C96Y} to generate AK-RPTC-RPTOR^{-/-} mice⁵⁸. To generate mice lacking TSC in RPTCs (WT-RPTC-TSC^{-/-}), we crossed mice containing two *loxP* sites flanking the open reading frame of the TSC gene (*Tsc1*^{fl/fl}; *Tsc2*^{tm2.1D3j/Mmjax}, #37154, Jackson Laboratories, Bar Harbor, ME) with the *iL1-sglt2-Cre* line¹⁰¹. To generate diabetic mice mutated for both CB₁R (homozygous) and TSC (heterozygous) in the RPTCs (AK-RPTC-CB₁R^{-/-}TSC^{+/-}), we crossed the AK-RPTC-CB₁R^{-/-} mice with the WT-RPTC-TSC^{-/-} mice.

At three weeks of age, littermates were divided into four groups according to their genotypes: WT-Cre⁻, WT-Cre⁺, AK-Cre⁻, and AK-Cre⁺. Cre⁻ or Cre⁺ refers to the presence or deletion of the gene of interest (*CB₁R*, *GLUT2*, *Raptor*, and *TSC*), respectively. All animals were homozygous for *flox*, except for TSC. The mice were monitored weekly for their blood glucose levels and body weight until they were sixteen weeks of age. Mice were subjected to a complete metabolic and kidney analysis. 24 h urine was collected one week before euthanasia using mouse

metabolic cages (CCS2000 Chiller System, Hatteras Instruments, NC, USA). At week 16, the mice were euthanized by a cervical dislocation under anesthesia, the kidneys and pancreases were removed and weighed, and samples were either snap-frozen or fixed in buffered 4% formalin. Trunk blood was collected for determining the biochemical parameters.

CB₁R activation in WT mice was done in 8-week-old, C57BL/6J male mice. WIN 55,212-2 (3 mg/kg), or a vehicle (Veh; 1% Tween80, 4% DMSO in saline) was injected *ip*, and after 6 h the mice were euthanized by a cervical dislocation under anesthesia, the kidneys were removed and were either snap-frozen or fixed in buffered 4% formalin.

Materials. ACEA, Wortmannin, WIN 55,212-2, and Rapamycin were purchased from Cayman Chemical (USA). PTX was purchased from Sigma-Aldrich (Israel). YM-254890 was purchased from AdipoGen (USA). JD5037 and DO34 were purchased from MedChemExpress (China).

Blood and urine biochemistry. Serum insulin and urine albumin were measured by ELISAs (Millipore and Bethyl Laboratories, respectively). Serum urea, urine/serum glucose, and creatinine were determined using a Cobas C-111 chemistry analyzer (Roche, Switzerland). Blood urea nitrogen (BUN) was calculated by the serum urea levels ($BUN\text{ mg/dL} = \text{Urea}\text{ mM} \times 2.801$). CCr was calculated using urine and serum creatinine levels ($CCr\text{ mL h}^{-1} = \text{Urine creatinine}\text{ mg/dL} \times \text{Urine volume/Serum creatinine}\text{ mg/dL} \times 24\text{ h}$). The urine levels of KIM-1 were measured by ELISA kit (R&D Systems, MN, USA).

Histopathological Analyses. Paraffin-embedded kidney and pancreas sections (5 μ m) from each group (5–6 animals per group) were stained with hematoxylin and eosin or Periodic Acid-Schiff (PAS), followed by hematoxylin staining. In addition, kidney sections were stained for collagen types I and III deposition by using Masson’s trichrome (Abcam, ab150686) staining according to the manufacturer’s procedures. Kidney and pancreas images were captured with a Zeiss AxioCam IC5 color camera mounted on a Zeiss Axio Scope.A1 light microscope, and taken from 10 random 40 \times fields of each animal. Mesangial expansion, glomerular, and Bowman’s space cross-sectional areas were quantified using ZEN imaging software (Zeiss, Germany). Masson’s trichrome positive areas were quantified using Image J software with a minimum of 10 random kidney images per mouse.

Fluorescence immunohistochemistry. Kidney sections were deparaffinized and hydrated. Heat-mediated antigen retrieval was performed with 10 mM citrate buffer pH 6.0 (Thermo Scientific, IL, USA). Unspecific antigens were blocked by incubating sections for 1 h with 5% goat serum (VE-S-1000, Vector Laboratories). The sections were stained with a Rabbit anti-LRP2 (ab76969, Abcam, 1:1000) antibody, followed by incubation with a Goat anti-Rabbit-AF488 antibody (ab150077, Abcam, 1:500). Sections were mounted with a mounting medium with DAPI (H-1200, Vector) and photographed using the LSM 700 imaging system (Zeiss). The relative fluorescent intensity (RFI) was measured using the ImageJ software (NIH, Bethesda, MD).

Cell culture. Human primary RPTCs (Lonza) were cultured in REGM BulletKit medium (Lonza), as described previously²⁵. HEK-293 cells were cultured in HG-DMEM supplemented with 10% fetal bovine serum and 100 IU/mL penicillin/streptomycin (Biological industries, Israel) at 37 °C in a humid atmosphere with 5% CO₂.

To test the effect of CB₁R blockade and its signaling pathways, hRPTCs or HEK-293 cells were cultured overnight with serum-free medium (SFM) REGM or DMEM low glucose (LG), respectively, supplemented with 0.1% BSA. One hour before exposing the cells to HG (30 mM) or activating CB₁R with arachidonyl-2'-chloroethylamide (ACEA; 10 μ M), the cells were pretreated with JD5037 (100 nM), DO34 (100 nM), Wortmannin (500 nM), Pertussis toxin (PTX; 100 ng/mL), YM254890 (1 μ M), or Rapamycin (100 nM) in SFM. Gradual time frames were used to detect the effect of the treatment on S6 and AKT phosphorylation as well as for eCB measurements (1 h), evaluating GLUT2 transcriptional activity (3 h), and assessing GLUT2 protein expression (24 h).

Immunofluorescence. hRPTCs were seeded on eight chambered coverglass (In Vitro Scientific) in REGM. The cells were starved overnight in SFM-REGM and pretreated for 1 h with JD5037 (100 nM) or rapamycin (100 nM) and then for an additional 24 h with HG (30 mM). Next, the cells were fixed with 4% PFA and permeabilized with 0.25% Triton x100. After an additional two hours of blocking in 2% BSA, cells were incubated overnight with Rabbit anti-GLUT2 (#AGT022, Alomone, 1:500) or Rabbit anti-SREBP1 (ab193318, Abcam, 1:500). Then, cells were incubated with Donkey anti-Rabbit-APC (#711-136-152, Jackson, 1:1000) or Goat anti-Rabbit-AF488 (ab150077, Abcam, 1:1000) secondary antibodies respectively, for 1 h and Hoechst for 15 minutes, and next photographed using a IX-73 fluorescent microscope (OLYMPUS) or a Confocal AIR microscope (Nikon). RFI was measured using Image J software.

Vectors. The hGLUT2 promoter 1043 bp site with the XhoI/HindIII restriction sites were amplified via PCR from hRPTC DNA and cloned into the multiple cloning region of the pGL3 luciferase reporter vector (Promega, USA), generating the pGL3-GLUT2 vector. The *Renilla* luciferase vector (Promega, USA) was used as a co-reporter vector and for expression control. The CB₁R-TK-d64 plasmid contained a short version of the CB₁R gene under the thymidine kinase (TK) promoter, enabling CB₁R to translocate to the plasma membrane more easily than the full-length CB₁R⁶⁴ (Supplementary Fig. 6).

GLUT2 transcription luciferase reporter assay. HEK-293 cells were transiently transfected using the Lipofectamine™ 3000 transfection reagent (Thermo Fisher Scientific, USA) with the pGL3-GLUT2 and *Renilla* vectors with/without the CB₁R-TK-d64 plasmid⁶⁴. One day following the transfection, cells were starved overnight in SFM and treated for 3 h with HG (30 mM) or CB₁R agonist-ACEA (10 μM), with/without 1 h pretreatment with JD5037 (100 nM) or Rapamycin (100 nM). The Dual-Glo Luciferase Assay System (Promega, USA) was used to detect GLUT2 promoter transcriptional activity. The Relative Response Ratio (RRR) was calculated for each treatment and compared to the control group.

Promoter-binding transcription-factor profiling assay. A list of ~120 TFs that can bind to the 1043 bp hGLUT2 promoter site was prepared using TFBIND software. A modified list of 47 relevant TFs was screened for their ability to bind to the hGLUT2 promoter using a promoter-binding TF profiling array (Signosis, USA). An assay was performed according to the manufacturer's instructions. Briefly, nuclear extract (NE) was isolated from 1 × 10⁷ hRPTCs, and treated/untreated with HG for 3 h, by using a nuclear protein extraction kit (Signosis, USA). The reaction mixture was prepared using 15 μL of the TF binding buffer, 3 μL of the probe, 10 μg of nuclear extract, and 5 μL of the hRPTC GLUT2 promoter fragment (1043 bp), and incubated at room temperature for 30 min to allow for the formation of the TF-DNA complex. Unbound probes were separated from the complex, whereas bound probes were eluted and then hybridized to the plate and incubated overnight at 42 °C. Bound probes were detected using an HRP-streptavidin conjugate incubated with the chemiluminescent substrate. Luminescence is reported as relative light units (RLUs) on the Multi-Mode Microplate Reader SpectraMax iD3 (Molecular Devices, USA).

Small interfering RNA treatment. Small interfering RNA (siRNA) transfection against SREBP1 (sc-36557, Santa Cruz) was performed in hRPTCs using the siRNA reagent system (sc-45064, Santa Cruz) according to the manufacturer's instructions.

In vivo micro PET-MRI scanning. Experiments were performed at the Wohl Institute for Translational Medicine at Hadassah Hebrew University Medical Center. PET-MRI images were acquired on a 7T 24 cm bore, a cryogen-free MR scanner based on the proprietary dry magnet technology (MR Solutions, Guildford, UK) with a 3-ring PET insert that uses the latest silicon photomultiplier (SiPM) technology¹⁰². The PET subsystem contains 24 detector heads arranged in three octagons of 116 mm in diameter. For MRI acquisition, a mouse quadrature RF volume coil was used. Mice were anesthetized with isoflurane vaporized with O₂. Isoflurane was used at 3.0% for induction and at 1.0–2.0% for maintenance. The mice were positioned on a heated bed, which allowed for continuous anesthesia and breathing rate monitoring. To determine the distribution of [¹⁸F]-FDG in mice, the tracer was injected into the tail vein (230 ± 30 mCi in 200 μL). Mice were subjected to 31 min dynamic PET scans; a homemade small catheter was inserted into the proximal tail vein and the tracer was injected after positioning the mouse in the micro-PET/MRI scanner. For dynamic scans, the acquired data were binned into 25 image frames (1 × 60, 6 × 10, 8 × 30, 5 × 60, and 4 × 300 s). During the PET, scans were acquired, T1 & T2; weighted coronal spin echo images were collected for anatomical evaluation. Coronal T1 weighted images were acquired using the following parameters: TR = 1100 ms, TE = 11 ms, echo spacing = 11 ms, FOV = 6 × 3 cm, slice thickness = 1 mm, 4 averages. Coronal T2-weighted images were acquired using the following parameters: TR = 4000 ms, TE = 45 ms, echo spacing = 15 ms, FOV = 6 × 3 cm, slice thickness = 1 mm, and 4 averages. Images were analyzed using VivoQuant pre-clinical image post-processing software (Invivo). PET-MRI raw data were processed using the standard software provided by the manufacturers. PET data were acquired in list-mode, histogrammed by Fourier re-binning, and reconstructed using the 3D-OSEM algorithm, with standard corrections for random coincidences, system response, and physical decay applied. The reconstructed PET images from the PET/MR scanner were quantitated using a measured system-specific ¹⁸F calibration factor to convert reconstructed count rates per voxel to activity concentrations (%ID/g). Manual tissue segmentation of kidneys, liver, muscle, inferior vena cava (IVC), and bladder was carried out on co-registered 3D MR images. The regions of interest were then used to calculate tissue radiotracer uptake from the reconstructed PET images.

Western blotting. Kidney or cell homogenates were prepared in a RIPA buffer (25 mM Tris-HCl pH 7.6, 150 mM NaCl, 1% NP-40, 1% sodium deoxycholate, 0.1% SDS). Kidney homogenates were prepared by using the BulletBlender® and zirconium oxide beads (Next Advanced, Inc., NY, USA). Protein concentrations

were measured with the Pierce™ BCA Protein Assay Kit (Thermo Scientific, IL, USA). Samples were resolved by SDS-PAGE (4–15% acrylamide, 150 V) and transferred to PVDF membranes using the Trans-Blot® Turbo™ Transfer System (Bio-Rad, CA). Membranes were then incubated for 1 h in 5% milk (in 1 × TBS-T) to block unspecific binding. Membranes were incubated overnight with Rabbit/Mouse anti-GLUT2 (#AGT022, Alomone, 1:1000; #720238, Invitrogen, 1:1000), Rabbit anti-phosphorylated-S6 ribosomal protein (#5364, Cell Signaling, 1:50000), Rabbit anti-phosphorylated-AKT (#9272, Cell Signaling, 1:500), Rabbit/Mouse anti-SREBP1 (#ab193318, #ab3259, Abcam, 1:500), Rabbit anti-SLC6A19 (#ab180516, Abcam, 1:500), Rabbit anti-SLC7A5 (#5347 S, Cell Signaling, 1:500), Rabbit anti-SGLT2 (#ab85626, Abcam) Goat anti-DAGLa (#ab81984, Abcam, 1:500), Rabbit anti-DAGLβ (#ab191159, Abcam, 1:1000), Rabbit anti-LRP2 (ab76969, Abcam, 1:500), and Rabbit anti-CB₁R (#301214, Immunogen, 1:500) antibodies (#ab97085, #ab98799, Abcam, 1:2500) were used for 1 h at room temperature, followed by chemiluminescence detection using Clarity™ Western ECL Blotting Substrate (Bio-Rad, CA), blot imaging was done using ChemiDoc™ Touch Imaging System (Bio-Rad, CA). Densitometry was quantified using Bio-Rad CFX Manager software. Quantification was normalized to Mouse anti-β actin antibody (#ab49900, Abcam, 1:30000) or Rabbit anti-VCP (#ab204290, Abcam, 1:1000). Phosphorylated S6 and AKT were normalized to total Rabbit anti-S6 ribosomal protein (#2217, Cell Signaling, 1:500) and Rabbit anti-total AKT (#4058, Cell Signaling, 1:500), respectively. Nuclear proteins were normalized to Mouse anti-Fibrillarin (#ab4566, Abcam, 1:500).

Real-time PCR. Total kidney or cell mRNA was extracted using Bio-Tri RNA lysis buffer (Bio-Lab, Israel), followed by DNase I treatment (Thermo Scientific, IL, USA), and reverse transcribed using the Iscript cDNA kit (Bio-Rad, CA). Real-time PCR was performed using iTaq Universal SYBR Green Supermix (Bio-Rad, CA) and the CFX connect ST system (Bio-Rad, CA). The primers used to detect mouse or human genes are listed in Supplementary Tables 1, 2. Mouse and human genes were normalized to *Ubc* or *RPLP*, respectively.

Sample preparation and endocannabinoid measurements by LC-MS/MS. The eCBs and related lipid measurements were performed in two independently laboratories. eCBs were extracted, purified, and quantified from RPTC lysates. In brief, A. (Tam Laboratory, Hebrew University) hRPTCs were scraped from the culture plates in ice-cold Tris Buffer, homogenized using sonication, and protein concentration was determined. Samples were then supplemented with an ice-cold Extraction buffer (1:1 Methanol/Tris Buffer+ Internal Standard) and Chloroform/Methanol (2:1), vortexed and centrifuged. The lower organic phase was transferred into borosilicate tubes; this step was repeated three times by adding ice-cold Chloroform to the samples and transferring the lower organic phase into the same borosilicate tubes. The samples were then dried and kept overnight in –80 °C, and then reconstitute with ice-cold Chloroform and Acetone then kept in –20 °C for 30 min and centrifuged to precipitate proteins. The supernatant was then dried and reconstituted in ice-cold LC/MS grade Methanol. LC-MS/MS was analyzed on an AB Sciex (Framingham, MA, USA) QTRAP® 6500 + mass spectrometer coupled with a Shimadzu (Kyoto, Japan) UHPLC System. Liquid chromatographic separation was obtained using 5 μL injections of samples onto a Kinetex 2.6 μm C18 (100°2.1 mm) column from Phenomenex (Torrance, CA, USA). The auto-sampler was set at 4 °C and the column was maintained at 40 °C during the entire analysis. Gradient elution mobile phases consisted of 0.1% formic acid in water (phase A) and 0.1% formic acid in acetonitrile (phase B). eCBs were detected in a positive ion mode using electron spray ionization (ESI) and the multiple reaction monitoring (MRM) mode of acquisition, using d₄-AEA as internal standard (IS). The collision energy (CE), declustering potential (DP), and collision cell exit potential (CXP) for the monitored transitions are given in Supplementary Table 5. The levels of AEA, 2-AG, OEA, PEA, and AA in samples were measured against standard curves, and normalized to the RPTC lysate protein concentration.

B. (Gertsch Laboratory, University of Bern) similar to Schuele et al.¹⁰³, the scraped hRPTCs were homogenized in 0.1 M FA by three times freeze-thaw cycles and sonification. The protein concentration was determined with an aliquot of the sample using BCA. The remaining homogenate was extracted in 9:1 ethyl acetate:hexane 0.1% FA solution (3:1 ratio organic to water part). After a drying the organic layer, the sample was reconstituted in 35 μL 80% acetonitrile and 10 μL was injected per measurement into the system. LC-MS/MS was conducted on an AB Sciex (Framingham, MA, USA) Triple Quad™ 5500 mass spectrometer coupled to a Shimadzu (Kyoto, Japan) UHPLC System. For the chromatographic separation, a C18 column (3 μm particle size; 2 × 50 mm, Dr. A. Maisch HPLC GmbH, Ammerbuch-Entringen, Germany) was used. In a positive mode, the mobile phase A was water containing 2 mM NH₄Ac 0.1% FA, and mobile phase B contained methanol and 2 mM NH₄Ac. In a negative mode, mobile phase A consisted of water 2 mM NH₄Ac 0.1% FA, and mobile phase B was acetonitrile 0.1% FA. The flow rate was set to 0.3 mL/min. eCBs were detected in a positive ion mode (for SAG, 2-AG, and ethanolamines) and AA in a negative mode using ESI and the MRM mode. The molecular ions and fragments for each compound are presented in Supplementary Table 5. Data acquisition and analysis were performed using Analyst software 1.6. For all analyses, a linear regression without weighing was applied. The levels of AEA, 2-AG, SAG, OEA, PEA, and AA in samples were

measured against standard curves, and normalized to the RPTC lysate protein concentration.

Sample preparation and amino acid measurement by LC-MS/MS. Amino acids were extracted, purified, and quantified from kidney lysates or from cultured hRPTCs. In brief, kidney samples were weighed, added with ice-cold methanol, sonicated to lysates, and centrifuged. The supernatant was diluted 1:10 in methanol with an internal standard (S-(2-Aminoethyl)-L-cysteine hydrochloride). hRPTCs were starved overnight in SFM DMEM F-12, w/o amino acids (USBiological, USA) and treated with/without JD5037 (100 nM) for 1 h. Then 0.05447 mg/mL L-Isoleucine, 0.05905 mg/mL L-Leucine, and 0.05285 mg/mL L-Valine were added to the medium and treated for 3 h; then the cells were lysed using a solvent containing methanol, acetonitrile, and water at a ratio of 5:3:2, respectively, with 5 μ M of the internal standard. LC-MS/MS analyses were conducted under reverse phase conditions on a Sciex (Framingham, MA, USA) QTRAP[®] 6500+ mass spectrometer coupled with a Shimadzu (Kyoto, Japan) UHPLC System. Liquid chromatographic separation was achieved using 5 μ L injections of samples onto an Intrada Amino Acids column 3 μ m (150*2 mm) from Imtakt Corp. (Kyoto, Japan). The autosampler was set at 10 °C and the column was maintained at 40 °C during the entire analysis. Gradient elution mobile phases consisted of 100 mM ammonium formate in water (phase A) and 0.1% formic acid in acetonitrile (phase B). Gradient elution (400 μ L/min) was held at 14% A for the first 3.75 min, followed by a linear increase towards 55% A in 5.5 min, a linear increase towards 100% A in 1 min, and held at 100% A for 6 min. Amino acids were detected in a positive ion mode using ESI and the Advanced Scheduled MRM mode of acquisition. The Turbo Spray IonDrive™ Turbo V source temperature was set at 650 °C, with the ion spray voltage at 5000 V. The curtain gas was set at 30.0 psi. The nebulizer gas (Gas 1) was set to 50 psi, and the turbo heater gas (Gas 2) was set to 60 psi. The CE, DP, and the CXP for the monitored transitions are presented in Supplementary Table 6. Data acquisition was performed on a Dell Optiplex XE2 computer using Analyst 1.7.1 and data was analyzed using Sciex OS Software. The levels of the amino acids in samples were measured against standard curves and normalized to the kidney weight.

Statistics. Values are expressed as the mean \pm SEM. Unpaired Two-tailed Student's t-test was used to determine the differences between two groups. Results in multiple groups were compared by one-way ANOVA followed by one-sided Tukey test, using GraphPad Prism v6 for Windows (San Diego, CA). Significance was set at $P < 0.05$.

Reporting summary. Further information on research design is available in the Nature Research Reporting Summary linked to this article.

Data availability

All data that support the findings of this study are available within the article, its Supplementary Information or Source Data files. Primers lists are provided in Supplementary Tables 1, 2 (in the Supplementary Information file). Uncropped gels are available in the Supplementary Information file. Source data are provided with this paper.

Received: 5 November 2020; Accepted: 25 February 2022;

Published online: 04 April 2022

References

- Lovic, D. et al. The growing epidemic of diabetes mellitus. *Curr. Vasc. Pharm.* **18**, 104–109 (2020).
- Gilbertson, D. T. et al. Projecting the number of patients with end-stage renal disease in the United States to the year 2015. *J. Am. Soc. Nephrol. JASN* **16**, 3736–3741 (2005).
- Declèves, A. E. & Sharma, K. New pharmacological treatments for improving renal outcomes in diabetes. *Nat. Rev. Nephrol.* **6**, 371–380 (2010).
- Zeni, L., Norden, A. G. W., Cancarini, G. & Unwin, R. J. A more tubulocentric view of diabetic kidney disease. *J. Nephrol.* **30**, 701–717 (2017).
- Gilbert, R. E. Proximal tubulopathy: Prime mover and key therapeutic target in diabetic kidney disease. *Diabetes* **66**, 791–800 (2017).
- Vallon, V. Glucose transporters in the kidney in health and disease. *Pflug. Arch.* **472**, 1345–1370 (2020).
- Makrides, V., Camargo, S. M. & Verrey, F. Transport of amino acids in the kidney. *Compr. Physiol.* **4**, 367–403 (2014).
- Wullschlegel, S., Loewith, R. & Hall, M. N. TOR signaling in growth and metabolism. *Cell* **124**, 471–484 (2006).
- Hirsch, S. & Tam, J. Cannabis: From a plant that modulates feeding behaviors toward developing selective inhibitors of the peripheral endocannabinoid system for the treatment of obesity and metabolic syndrome. *Toxins* **11**, 275 (2019).
- DiPatrizio, N. V. & Piomelli, D. The thrifty lipids: Endocannabinoids and the neural control of energy conservation. *Trends Neurosci.* **35**, 403–411 (2012).
- Tam, J. The emerging role of the endocannabinoid system in the pathogenesis and treatment of kidney diseases. *J. Basic Clin. Physiol. Pharmacol.* **27**, 267–276 (2016).
- Hinden, L. & Tam, J. Do Endocannabinoids regulate glucose reabsorption in the kidney? *Nephron* **143**, 24–27 (2019).
- Grahammer, F., Wanner, N. & Huber, T. B. mTOR controls kidney epithelia in health and disease. *Nephrol. Dial. Transpl.* **29**, i9–i18 (2014).
- Fantus, D., Rogers, N. M., Grahammer, F., Huber, T. B. & Thomson, A. W. Roles of mTOR complexes in the kidney: Implications for renal disease and transplantation. *Nat. Rev. Nephrol.* **12**, 587–609 (2016).
- Lee, Y. H. et al. Empagliflozin attenuates diabetic tubulopathy by improving mitochondrial fragmentation and autophagy. *Am. J. Physiol. Ren. Physiol.* **317**, F767–F780 (2019).
- Yasuda-Yamahara, M., Kume, S. & Maegawa, H. Roles of mTOR in diabetic kidney disease. *Antioxidants* **10**, 321 (2021).
- Barutta, F. et al. Cannabinoid receptor 1 blockade ameliorates albuminuria in experimental diabetic nephropathy. *Diabetes* **59**, 1046–1054 (2010).
- Jenkin, K. A., McAinch, A. J., Zhang, Y., Kelly, D. J. & Hryciw, D. H. Elevated cannabinoid receptor 1 and G protein-coupled receptor 55 expression in proximal tubule cells and whole kidney exposed to diabetic conditions. *Clin. Exp. Pharmacol. Physiol.* **42**, 256–262 (2015).
- Nam, D. H. et al. Blockade of cannabinoid receptor 1 improves insulin resistance, lipid metabolism, and diabetic nephropathy in db/db mice. *Endocrinology* **153**, 1387–1396 (2012).
- Jourdan, T. et al. Overactive cannabinoid 1 receptor in podocytes drives type 2 diabetic nephropathy. *Proc. Natl. Acad. Sci. USA* **111**, E5420–E5428 (2014).
- Udi, S. et al. Proximal tubular cannabinoid-1 receptor regulates obesity-induced CKD. *J. Am. Soc. Nephrol.* **28**, 3518–3532 (2017).
- Lim, J. C. et al. Cannabinoid receptor 1 mediates high glucose-induced apoptosis via endoplasmic reticulum stress in primary cultured rat mesangial cells. *Am. J. Physiol. Ren. Physiol.* **301**, F179–F188 (2011).
- Lin, C. L. et al. Cannabinoid receptor 1 disturbance of PPAR γ 2 augments hyperglycemia induction of mesangial inflammation and fibrosis in renal glomeruli. *J. Mol. Med.* **92**, 779–792 (2014).
- Jourdan, T. et al. Cannabinoid-1 receptor deletion in podocytes mitigates both glomerular and tubular dysfunction in a mouse model of diabetic nephropathy. *Diabetes, Obes. Metab.* **20**, 698–708 (2018).
- Hinden, L. et al. Modulation of renal GLUT2 by the cannabinoid-1 receptor: Implications for the treatment of diabetic nephropathy. *J. Am. Soc. Nephrol. JASN* **29**, 434–448 (2018).
- Chen, X., Yang, Y., Liu, C., Chen, Z. & Wang, D. Astragaloside IV ameliorates high glucose-induced renal tubular epithelial-mesenchymal transition by blocking mTORC1/p70S6K signaling in HK2 cells. *Int. J. Mol. Med.* **43**, 709–716 (2019).
- Lu, Q. et al. ROS induces epithelial-mesenchymal transition via the TGF- β 1/PI3K/Akt/mTOR pathway in diabetic nephropathy. *Exp. Ther. Med.* **17**, 835–846 (2019).
- Wu, C. et al. Klotho restraining Egr1/TLR4/mTOR axis to reducing the expression of fibrosis and inflammatory cytokines in high glucose cultured rat mesangial cells. *Exp. Clin. Endocrinol. Diabetes* **127**, 630–640 (2018).
- Lei, J., Zhao, L., Zhang, Y., Wu, Y. & Liu, Y. High glucose-induced podocyte injury involves activation of mammalian target of rapamycin (mTOR)-induced endoplasmic reticulum (ER) stress. *Cell Physiol. Biochem.* **45**, 2431–2443 (2018).
- Lu, Q. et al. The mTOR promotes oxidative stress-induced apoptosis of mesangial cells in diabetic nephropathy. *Mol. Cell Endocrinol.* **473**, 31–43 (2018).
- Das, F., Ghosh-Choudhury, N., Venkatesan, B., Kasinath, B. S. & Ghosh Choudhury, G. PDGF receptor-beta uses Akt/mTORC1 signaling node to promote high glucose-induced renal proximal tubular cell collagen I (alpha2) expression. *Am. J. Physiol. Ren. Physiol.* **313**, F291–F307 (2017).
- Gong, Q. & Hou, F. Silencing of angiotensin II type-1 receptor inhibits high glucose-induced epithelial-mesenchymal transition in human renal proximal tubular epithelial cells via inactivation of mTOR/p70S6K signaling pathway. *Biochem. Biophys. Res. Commun.* **469**, 183–188 (2016).
- Inoki, K. et al. mTORC1 activation in podocytes is a critical step in the development of diabetic nephropathy in mice. *J. Clin. Invest.* **121**, 2181–2196 (2011).
- Godel, M. et al. Role of mTOR in podocyte function and diabetic nephropathy in humans and mice. *J. Clin. Invest.* **121**, 2197–2209 (2011).
- Bera, A. et al. Reciprocal regulation of miR-214 and PTEN by high glucose regulates renal glomerular mesangial and proximal tubular epithelial cell hypertrophy and matrix expansion. *Am. J. Physiol. Cell Physiol.* **313**, C430–C447 (2017).
- Lu, Q. et al. Quercetin inhibits the mTORC1/p70S6K signaling-mediated renal tubular epithelial-mesenchymal transition and renal fibrosis in diabetic nephropathy. *Pharm. Res.* **99**, 237–247 (2015).

37. Dey, N. et al. MicroRNA-21 orchestrates high glucose-induced signals to TOR complex 1, resulting in renal cell pathology in diabetes. *J. Biol. Chem.* **286**, 25586–25603 (2011).
38. Kuwagata, S. et al. MicroRNA148b-3p inhibits mTORC1-dependent apoptosis in diabetes by repressing TNFR2 in proximal tubular cells. *Kidney Int.* **90**, 1211–1225 (2016).
39. Kume, S., Koya, D., Uzu, T. & Maegawa, H. Role of nutrient-sensing signals in the pathogenesis of diabetic nephropathy. *Biomed. Res. Int.* **2014**, 315494 (2014).
40. Blazquez, C. et al. The CB(1) cannabinoid receptor signals striatal neuroprotection via a PI3K/Akt/mTORC1/BDNF pathway. *Cell Death Differ.* **22**, 1618–1629 (2015).
41. Puighermanal, E. et al. Cannabinoid modulation of hippocampal long-term memory is mediated by mTOR signaling. *Nat. Neurosci.* **12**, 1152–1158 (2009).
42. Gomez, O. et al. Cannabinoid receptor agonists modulate oligodendrocyte differentiation by activating PI3K/Akt and the mammalian target of rapamycin (mTOR) pathways. *Br. J. Pharm.* **163**, 1520–1532 (2011).
43. Garcia-Rincon, D. et al. Contribution of altered endocannabinoid system to overactive mTORC1 signaling in focal cortical dysplasia. *Front. Pharm.* **9**, 1508 (2018).
44. Puighermanal, E. et al. Dissociation of the pharmacological effects of THC by mTOR blockade. *Neuropsychopharmacology* **38**, 1334–1343 (2013).
45. Bermudez-Silva, F. J. et al. The cannabinoid CB1 receptor and mTORC1 signalling pathways interact to modulate glucose homeostasis in mice. *Dis. Model Mech.* **9**, 51–61 (2016).
46. Senin, L. L. et al. The gastric CB1 receptor modulates ghrelin production through the mTOR pathway to regulate food intake. *PLoS One* **8**, e80339 (2013).
47. Bian, C., Bai, B., Gao, Q., Li, S. & Zhao, Y. 17beta-estradiol regulates glucose metabolism and insulin secretion in rat islet beta cells through GPER and Akt/mTOR/GLUT2 pathway. *Front. Endocrinol.* **10**, 531 (2019).
48. Larkins, R. G. & Dunlop, M. E. The link between hyperglycaemia and diabetic nephropathy. *Diabetologia* **35**, 499–504 (1992).
49. Wolf, G. & Thaiss, F. Hyperglycaemia-pathophysiological aspects at the cellular level. *Nephrol., Dialysis, Transplant.: Off. Publ. Eur. Dialysis Transpl. Assoc. - Eur. Ren. Assoc.* **10**, 1109–1112 (1995).
50. Thorens, B., Wu, Y. J., Leahy, J. L. & Weir, G. C. The loss of GLUT2 expression by glucose-unresponsive beta cells of db/db mice is reversible and is induced by the diabetic environment. *J. Clin. Invest.* **90**, 77–85 (1992).
51. Jorns, A., Tiedge, M., SICKEL, E. & Lenzen, S. Loss of GLUT2 glucose transporter expression in pancreatic beta cells from diabetic Chinese hamsters. *Virchows Arch.* **428**, 177–185 (1996).
52. Orci, L. et al. Evidence that down-regulation of beta-cell glucose transporters in non-insulin-dependent diabetes may be the cause of diabetic hyperglycemia. *Proc. Natl Acad. Sci. USA* **87**, 9953–9957 (1990).
53. Rahmoune, H. et al. Glucose transporters in human renal proximal tubular cells isolated from the urine of patients with non-insulin-dependent diabetes. *Diabetes* **54**, 3427–3434 (2005).
54. Chin, E. et al. Changes in facilitative glucose transporter messenger ribonucleic acid levels in the diabetic rat kidney. *Endocrinology* **138**, 1267–1275 (1997).
55. Marks, J., Carvou, N. J., Debnam, E. S., Srail, S. K. & Unwin, R. J. Diabetes increases facilitative glucose uptake and GLUT2 expression at the rat proximal tubule brush border membrane. *J. Physiol.* **553**, 137–145 (2003).
56. Chichger, H. et al. Experimental type II diabetes and related models of impaired glucose metabolism differentially regulate glucose transporters at the proximal tubule brush border membrane. *Exp. Physiol.* **101**, 731–742 (2016).
57. Thorens, B. Glucose transporters in the regulation of intestinal, renal, and liver glucose fluxes. *Am. J. Physiol.* **270**, G541–G553 (1996).
58. Kogot-Levin, A. et al. Proximal tubule mTORC1 is a central player in the pathophysiology of diabetic nephropathy and its correction by SGLT2 inhibitors. *Cell Rep.* **32**, 107954 (2020).
59. Dalton, G. D. & Howlett, A. C. Cannabinoid CB1 receptors transactivate multiple receptor tyrosine kinases and regulate serine/threonine kinases to activate ERK in neuronal cells. *Br. J. Pharm.* **165**, 2497–2511 (2012).
60. Gomez del Pulgar, T., Velasco, G. & Guzman, M. The CB1 cannabinoid receptor is coupled to the activation of protein kinase B/Akt. *Biochem. J.* **347**, 369–373 (2000).
61. Mallipeddi, S., Janero, D. R., Zvonok, N. & Makriyannis, A. Functional selectivity at G-protein coupled receptors: Advancing cannabinoid receptors as drug targets. *Biochem. Pharm.* **128**, 1–11 (2017).
62. Lauckner, J. E., Hille, B. & Mackie, K. The cannabinoid agonist WIN55,212-2 increases intracellular calcium via CB1 receptor coupling to Gq/11 G proteins. *Proc. Natl Acad. Sci. USA* **102**, 19144–19149 (2005).
63. Sampaio, L. S. et al. The endocannabinoid system in renal cells: regulation of Na(+) transport by CB1 receptors through distinct cell signalling pathways. *Br. J. Pharm.* **172**, 4615–4625 (2015).
64. Andersson, H., D'Antona, A. M., Kendall, D. A., Von Heijne, G. & Chin, C. N. Membrane assembly of the cannabinoid receptor 1: Impact of a long N-terminal tail. *Mol. Pharm.* **64**, 570–577 (2003).
65. David-Silva, A. et al. Hepatocyte nuclear factors 1alpha/4alpha and forkhead box A2 regulate the solute carrier 2A2 (Slc2a2) gene expression in the liver and kidney of diabetic rats. *Life Sci.* **93**, 805–813 (2013).
66. Freitas, H. S. et al. SLC2A2 gene expression in kidney of diabetic rats is regulated by HNF-1alpha and HNF-3beta. *Mol. Cell Endocrinol.* **305**, 63–70 (2009).
67. Kim, J. & Guan, K. L. mTOR as a central hub of nutrient signalling and cell growth. *Nat. Cell Biol.* **21**, 63–71 (2019).
68. Deutsch, D. G. et al. Production and physiological actions of anandamide in the vasculature of the rat kidney. *J. Clin. Invest.* **100**, 1538–1546 (1997).
69. Koura, Y. et al. Anandamide decreases glomerular filtration rate through predominant vasodilation of efferent arterioles in rat kidneys. *J. Am. Soc. Nephrol.: JASN* **15**, 1488–1494 (2004).
70. Sampaio, L. S. et al. Experimental ischemia/reperfusion model impairs endocannabinoid signaling and Na(+)/K(+) ATPase expression and activity in kidney proximal tubule cells. *Biochem. Pharm.* **154**, 482–491 (2018).
71. Grahammer, F. et al. mTOR regulates endocytosis and nutrient transport in proximal tubular cells. *J. Am. Soc. Nephrol.* **28**, 230–241 (2017).
72. Kempe, D. S. et al. Rapamycin-induced phosphaturia. *Nephrol., Dialysis, Transplant.: Off. Publ. Eur. Dialysis Transpl. Assoc. - Eur. Ren. Assoc.* **25**, 2938–2944 (2010).
73. Khandelwal, P. et al. Fanconi syndrome and neonatal diabetes: Phenotypic heterogeneity in patients with GLUT2 defects. *CEN Case Rep.* **7**, 1–4 (2018).
74. Brown, G. K. Glucose transporters: Structure, function, and consequences of deficiency. *J. Inherit. Metab. Dis.* **23**, 237–246 (2000).
75. Tam, J. et al. Peripheral cannabinoid-1 receptor inverse agonism reduces obesity by reversing leptin resistance. *Cell Metab.* **16**, 167–179 (2012).
76. Jenkin, K. A. et al. Chronic administration of AM251 improves albuminuria and renal tubular structure in obese rats. *J. Endocrinol.* **225**, 113–124 (2015).
77. Javed, K. & Broer, S. Mice lacking the intestinal and renal neutral amino acid transporter SLC6A19 demonstrate the relationship between dietary protein intake and amino acid malabsorption. *Nutrients* **11**, 2024 (2019).
78. Jiang, Y. et al. Mice lacking neutral amino acid transporter B(0)AT1 (Slc6a19) have elevated levels of FGF21 and GLP-1 and improved glycaemic control. *Mol. Metab.* **4**, 406–417 (2015).
79. Bauch, C., Forster, N., Löffing-Cueni, D., Summa, V. & Verrey, F. Functional cooperation of epithelial heteromeric amino acid transporters expressed in madin-darby canine kidney cells. *J. Biol. Chem.* **278**, 1316–1322 (2003).
80. Milkereit, R. et al. LAPT4b recruits the LAT1-4F2hc Leu transporter to lysosomes and promotes mTORC1 activation. *Nat. Commun.* **6**, 7250 (2015).
81. Zibolka, J. et al. Influence of cannabinoid receptor deficiency on parameters involved in blood glucose regulation in mice. *Int. J. Mol. Sci.* **21**, 3168 (2020).
82. Hegyi, Z. et al. CB1 receptor activation induces intracellular Ca(2+) mobilization and 2-arachidonoylglycerol release in rodent spinal cord astrocytes. *Sci. Rep.* **8**, 10562 (2018).
83. Hermann, H. et al. Dual effect of cannabinoid CB1 receptor stimulation on a vanilloid VR1 receptor-mediated response. *Cell. Mol. Life Sci.: CMLS* **60**, 607–616 (2003).
84. Jun, H. et al. In vivo and in vitro effects of SREBP-1 on diabetic renal tubular lipid accumulation and RNAi-mediated gene silencing study. *Histochem. Cell Biol.* **131**, 327–345 (2009).
85. Hao, J. et al. High-fat diet causes increased serum insulin and glucose which synergistically lead to renal tubular lipid deposition and extracellular matrix accumulation. *Br. J. Nutr.* **107**, 74–85 (2012).
86. Yang, W. et al. Ectopic lipid accumulation: Potential role in tubular injury and inflammation in diabetic kidney disease. *Clin. Sci.* **132**, 2407–2422 (2018).
87. Hao, J. et al. PI3K/Akt pathway mediates high glucose-induced lipogenesis and extracellular matrix accumulation in HKC cells through regulation of SREBP-1 and TGF-beta1. *Histochem. Cell Biol.* **135**, 173–181 (2011).
88. Takashima, M., Ogawa, W., Emi, A. & Kasuga, M. Regulation of SREBP1c expression by mTOR signaling in hepatocytes. *Kobe J. Med. Sci.* **55**, E45–E52 (2009).
89. Yecies, J. L. et al. Akt stimulates hepatic SREBP1c and lipogenesis through parallel mTORC1-dependent and independent pathways. *Cell Metab.* **14**, 21–32 (2011).
90. Norrmen, C. et al. mTORC1 controls PNS myelination along the mTORC1-RXRgamma-SREBP-lipid biosynthesis axis in Schwann cells. *Cell Rep.* **9**, 646–660 (2014).
91. Im, S. S. et al. Glucose-stimulated upregulation of GLUT2 gene is mediated by sterol response element-binding protein-1c in the hepatocytes. *Diabetes* **54**, 1684–1691 (2005).
92. Matias, I. et al. Regulation, function, and dysregulation of endocannabinoids in models of adipose and beta-pancreatic cells and in obesity and hyperglycemia. *J. Clin. Endocrinol. Metab.* **91**, 3171–3180 (2006).
93. Thorens, B., Guillam, M. T., Beermann, F., Burcelin, R. & Jaquet, M. Transgenic repression of GLUT1 or GLUT2 in pancreatic beta cells rescues GLUT2-null mice from early death and restores normal glucose-stimulated insulin secretion. *J. Biol. Chem.* **275**, 23751–23758 (2000).

94. Grunert, S. C., Schwab, K. O., Pohl, M., Sass, J. O. & Santer, R. Fanconi-Bickel syndrome: GLUT2 mutations associated with a mild phenotype. *Mol. Genet. Metab.* **105**, 433–437 (2012).
95. Cohen, M. et al. Live imaging of GLUT2 glucose-dependent trafficking and its inhibition in polarized epithelial cysts. *Open Biol.* **4**, 140091 (2014).
96. Song, P. et al. Knockout of Na(+)-glucose cotransporter SGLT1 mitigates diabetes-induced upregulation of nitric oxide synthase NOS1 in the macula densa and glomerular hyperfiltration. *Am. J. Physiol. Ren. Physiol.* **317**, F207–F217 (2019).
97. Dominguez, J. H., Camp, K., Maianu, L., Feister, H. & Garvey, W. T. Molecular adaptations of GLUT1 and GLUT2 in renal proximal tubules of diabetic rats. *Am. J. Physiol.* **266**, F283–F290 (1994).
98. Umino, H. et al. High basolateral glucose increases sodium-glucose cotransporter 2 and reduces sirtuin-1 in renal tubules through glucose transporter-2 detection. *Sci. Rep.* **8**, 6791 (2018).
99. Kilkenny, C. et al. Animal research: Reporting in vivo experiments: the ARRIVE guidelines. *Br. J. Pharmacol.* **160**, 1577–1579 (2010).
100. Seyer, P. et al. Hepatic glucose sensing is required to preserve beta cell glucose competence. *J. Clin. Invest.* **123**, 1662–1676 (2013).
101. Rubera, I. et al. Specific Cre/Lox recombination in the mouse proximal tubule. *J. Am. Soc. Nephrol. JASN* **15**, 2050–2056 (2004).
102. Courteau, A. et al. Performance evaluation and compatibility studies of a compact preclinical scanner for simultaneous PET/MR imaging at 7 Tesla. *IEEE Trans. Med. Imaging* **40**, 205–217 (2021).
103. Khan, S. et al. Kidney proximal tubule lipoapoptosis is regulated by fatty acid transporter-2 (FATP2). *J. Am. Soc. Nephrol.* **29**, 81–91 (2018).

Acknowledgements

We would like to thank Prof. Boaz Tirosh for his critical advice on mTORC1 signaling, and Dr. Dinorah Barasch for her technical assistance in LC-MS/MS analysis. This work was supported by an ERC-2015-StG grant (#676841), an Israel Science Foundation (ISF) grant (#158/18), and a JDRF grant (1-INO-2022-1128-A-N) to J.T. The work of G.S. was supported by the National Research, Development and Innovation Office grant NKFI-6/FK_124038.

Author contributions

L.H., M.A., and S.H. conducted the experiments and analyzed the data. A.N., S.G., and J.G. conducted the LC-MS/MS analyses. A.K.L. and G.L. assisted with the animal

experiments. G.S. provided experimental reagents. B.T. provided the GLUT2^{fl/fl} mice. R.A. performed the PET-MRI studies. L.H. and J.T. designed and supervised the experiments and wrote the manuscript. All co-authors contributed to writing the manuscript.

Competing interests

The authors declare no competing interests.

Additional information

Supplementary information The online version contains supplementary material available at <https://doi.org/10.1038/s41467-022-29124-8>.

Correspondence and requests for materials should be addressed to Joseph Tam.

Peer review information *Nature Communications* thanks Vincenzo Di Marzo, Daisuke Koya, and the other, anonymous, reviewer(s) for their contribution to the peer review of this work. Peer reviewer reports are available.

Reprints and permission information is available at <http://www.nature.com/reprints>

Publisher's note Springer Nature remains neutral with regard to jurisdictional claims in published maps and institutional affiliations.



Open Access This article is licensed under a Creative Commons Attribution 4.0 International License, which permits use, sharing, adaptation, distribution and reproduction in any medium or format, as long as you give appropriate credit to the original author(s) and the source, provide a link to the Creative Commons license, and indicate if changes were made. The images or other third party material in this article are included in the article's Creative Commons license, unless indicated otherwise in a credit line to the material. If material is not included in the article's Creative Commons license and your intended use is not permitted by statutory regulation or exceeds the permitted use, you will need to obtain permission directly from the copyright holder. To view a copy of this license, visit <http://creativecommons.org/licenses/by/4.0/>.

© The Author(s) 2022